# How the cortico-thalamic feedback affects the EEG power spectrum over frontal and occipital regions during propofol-induced anaesthetic sedation

Meysam Hashemi, Axel Hutt, Jamie Sleigh

# How the cortico-thalamic feedback affects the EEG power spectrum over frontal and occipital regions during propofol-induced anaesthetic sedation

Meysam Hashemi[a,*], Axel Hutt[a], Jamie Sleigh[b]

[a] *INRIA CR Nancy - Grand Est, Team Neurosys, 54602 Villers-les-Nancy, France*
[b] *University of Auckland, Hamilton, New Zealand*

**Abstract**

Increasing concentrations of the anaesthetic agent propofol initially induces sedation before achieving full general anaesthesia. The characteristic changes in electroencephalographic (EEG) rhythms include increased activity in the $\delta-$ (1-4 Hz) and $\alpha-$ (8-12 Hz) frequency bands over the frontal region, but increased $\delta-$ and decreased $\alpha-$activity over the occipital region. It is known that the cortex, the thalamus, and the thalamo-cortical feedback loop contribute to some degree to the propofol-induced changes in the EEG power spectrum. However the precise role of each structure to the dynamics of the EEG is unknown. In this paper we apply a neuronal population model of a single thalamo-cortical module to reproduce the power spectrum changes in EEG during propofol-induced anaesthesia sedation. Based on recent experimental data, the effect of propofol is modelled as an increase in inhibitory synaptic response amplitude and decay time constant in thalamo-cortical relay cells while cortical inhibition is neglected.

The model reproduces the power spectrum features observed experimentally both in frontal and occipital electrodes. Moreover a detailed analysis of the model indicates the importance of multiple resting states in brain activity. The work suggests that the $\alpha-$activity originates from the cortico-thalamic relay interaction, whereas the emergence of $\delta-$activity results from the full cortico-reticular-relay-cortical feedback loop with a prominent enforced thalamic reticular-relay interaction. This model suggests an essential role of synaptic GABAergic receptors at

*Corresponding Author: Meysam Hashemi, Address: INRIA CR Nancy - Grand Est, Team Neurosys, 615 rue du Jardin Botanique, 54602 Villers-les-Nancy, France.
Tel.: +33 (0)3 54 95 84 55
*Email address:* meysam.hashemi@inria.fr (Meysam Hashemi)

relay neurons and, more generally, for the thalamus in the generation of both the $\alpha-$ and the $\delta-$ EEG patterns that are seen during propofol anaesthesia sedation.

*Keywords:* Anaesthesia sedation, EEG, Propofol, Thalamo-cortical model

## 1. Introduction

General anaesthesia (GA) is a reversible medical procedure that is commonly induced by the administration of a combination of anaesthetic agents (AAs) to induce amnesia, sedation, and hypnosis (loss of consciousness) in patients. There are differing definitions of general anaesthesia, but phenomena such as analgesia, muscle relaxation and anxiolysis should be included, in addition to the most obvious effect of loss of consciousness (Rudolph and Antkowiak, 2004).

Although GA is used to allow most surgery, its precise underlying mechanisms are not yet fully understood and the molecular action of AAs on patients remain to be elucidated.

Propofol, an emulsion formulation of 2,6-di-isopropylphenol, is a short-acting, intravenously administered hypnotic agent; and is in widespread use for sedation and general anaesthesia because of its relatively fast onset and offset, and anti-emetic effects (San-juan et al., 2010).

Recent research has revealed possible molecular sites and neuronal pathways for the action of the anaesthetic propofol in the human brain. In vivo extracellular recordings have demonstrated that propofol suppresses field potentials in the rat thalamus and cortex (Antkowiak, 2002). Although some reports put emphasis on more prominent effects in the cortex, the cortical suppression may, in fact, be secondary to anaesthetic action on projection neurons located elsewhere in the brain, especially in the thalamus. Also several lines of evidence indicate that thalamus and thalamic neuronal circuits are important target-sites for propofol to produce hypnotic effects (Franks, 2008; Ying and Goldstein, 2001). Moreover experimental observations strongly suggest that reticular thalamic neurons (RTN) are a major source of inhibition to relay neurons; and are thus a critical structure for the effect of propofol in thalamic circuits (Byoung-Kyong, 2010; Ying and Goldstein, 2005b). These findings motivated us to neglect the propofol effect in cortical cells and concentrate just on the effect of propofol in thalamic neurons - in contrast to previous studies, e.g. Hindriks and van Putten (2012); Steyn-Ross et al. (2004); Bojak and Liley (2005). This assumption points out the importance of the thalamus and weakens the impact of the cortex for major neural effects under anaesthesia sedation.

For clinically relevant concentration of propofol specific changes in electroencephalogram (EEG) rhythms can be observed experimentally. These observations include an increase in power in the $\alpha-$ (at about 10 Hz) and $\delta-$ (at about 3 Hz) frequency band over the frontal head region, accompanied by decreased $\alpha-$power peak, and an increase in $\delta-$activity over the occipital sites (Murphy et al., 2011; Ching et al., 2010; Feshchenko et al., 2004; Hazeaux et al., 1987). It has been shown that at sedative concentrations, propofol attenuates posterior $\alpha-$ power and increases frontal $\beta$ and total power (Vijayan et al., 2013; Cimenser et al., 2011; Gugino et al., 2001) that is commonly termed *anteriorization*. Deeper sedation is associated with a frontal increase in $\alpha-$, $\delta$, and $\theta-$power. With the loss of consciousness frontal power further increases within every frequency band (Gugino et al., 2001).

Ching et al. (2010) have developed a thalamo-cortical model that suggests the importance of the thalamus in rhythmic activity in the frontal EEG. They have shown that synchronous frontal $\alpha-$activity in the EEG is the result of recruitment of some subset of the thalamic network into the cortical rhythm. This is in contrast to the theory of thalamic deactivation during general anaesthesia. A recent study (Vijayan et al., 2013) suggests that reduction in hyperpolarization-activated current ($I_h$) silences bursting of a subset of thalamo-cortical cells leading to suppression of occipital $\alpha-$activity. Their work suggests that increased GABAergic inhibition onto thalamo-cortical cells result into an $\alpha-$timescale that is reinforced by reciprocal thalamo-cortical feedback which is supposed to be responsible for emerged frontal $\alpha-$activity.

Alkire et al. (2000) proposed that thalamo-cortical cells are involved in producing anaesthetic induced $\delta-$activity in which the firing mode of thalamic relay neurons shifts from a tonic to a burst pattern by decreased excitation, thereby producing $\delta-$activity.

The EEG represents the neural activity of thousands or millions of spatially oriented pyramidal neurons of the cortex (Nunez and Srinivasan, 2006). By virtue of this large number of neurons, it is reasonable physiologically to model EEG by considering spatiotemporal neural activity of populations using a mean-field approximation (Nunez, 1981; Jirsa and Haken, 1996; Liley et al., 2002; Pinotsis et al., 2012; Freestone et al., 2011). This description involves averages of synaptic and neuron activity over a population in small spatial patches and short time windows (Nunez, 1974; Wilson and Cowan, 1973).

Most of the previous theoretical studies on anaesthetic effects apply a mean-field model to explain various features in EEG data recorded during general anaes-

thesia (Liley and Bojak, 2005; Bojak and Liley, 2005; Steyn-Ross et al., 1999, 2001a,b; Molaee-Ardekani et al., 2007; Hindriks and van Putten, 2012; Hutt and Longtin, 2009; Foster et al., 2008). These theoretical studies are based on various extensions of the model of Liley et al. (1999), Wilson and Cowan (1973) and Amari (1977) including excitatory and inhibitory synapses and neurons. The present work considers a neural population model based on a recently developed neural field model (Hutt and Longtin, 2009). It includes a cortical population synaptically connected to a thalamic reticular and relay neuron population by delayed thalamo-cortical axonal fibres. The model takes into account anaesthetic action at inhibitory GABAergic synaptic receptors in thalamic relay cells while, in the major part of the study, neglecting in anaesthetic action in the cortex.

The study provides evidence that thalamic GABAergic synaptic inhibition is one of the key actions inducing the characteristic changes in the $\delta-$ and $\alpha-$frequency ranges under propofol-induced sedation. Moreover, the work suggests the existence of two major cortico-thalamic sub-circuits that generate $\delta-$ and $\alpha-$spectral power peaks. To our best knowledge this is the first study that reproduces the EEG changes over frontal and occipital areas by neural populations model of a thalamo-cortical system.

The next section presents the acquisition procedure of experimental EEG under anaesthesia and the neural population model involving the population network, the anaesthetic action and the analysis steps to be taken. Then, we present the power spectra of experimental EEG in frontal and occipital electrodes and show that the neural population model proposed reproduces very well the characteristic spectral features in the $\delta-$ and $\alpha-$band subjected to the propofol concentration. The subsequent analysis of the model reveals the importance of multiple resting states and the presence of effective sub-circuits generating the spectral features in $\delta-$ and $\alpha-$frequency bands.

## 2. Materials and methods

### *2.1. EEG recordings during anaesthesia sedation*

We reanalysed previously-obtained experimental data from subjects that had been given a short propofol anaesthetic. The details of the methods can be found in (Johnson et al., 2003). In brief, after obtaining regional ethical committee approval and written informed consent, five healthy subjects (mean age 27.7 yrs, four males) were studied. They were on no psychoactive drugs and had been starved for at least 6 hours prior to the study. They were monitored and managed as per clinical anaesthesia, according to the Australia and New Zealand College of Anaesthetists best practice guidelines. The induction consisted of an intravenous infusion of propofol at 1500 mg/hr until the subject no longer responded to verbal command (typically this occurred about 5 minutes into the infusion). At this point the propofol infusion was stopped and the subject allowed to recover spontaneously. The duration of loss of consciousness was also about 5 minutes. The estimated effect-site concentrations of propofol were calculated using standard population-based pharmacokinetic models.

### *2.2. EEG acquisition and Data Processing*

The high-density EEG was acquired using the Electrical Geodesics 128 channel Ag/AgCl electrode system (Eugene, CO, USA) referenced to Cz. Electrode impedances were below 30 KOhm (100 MOhm input impedance amplifier), and a custom built head support device was used so as to allow recording of occipital channels when supine. The sampling frequency was 250 Hz, with a 0.1-100 Hz analogue band pass filter, and A-D conversion was at 12 bits precision. The EEG data were re-referenced to a grand mean, and band-pass filtered using 3-rd order Butterworth filters 0.2-45 Hz to eliminate line-noise. A Whittaker filter was applied to reduce movement and blink artifacts. The power in each frequency was expressed in decibels, and obtained applying a short-time Fourier transform using the "spectrogram.m" Matlab (Mathworks, Natick, Massachusetts, USA) function with a moving window of 2 sec and 1 sec overlap.

*Thalamo-cortical model*

The body of the work is based on a population-level model of a single thalamo-cortical module that is illustrated in Fig. 1. This module consists of four different populations of neurons (Rennie et al., 2002; Robinson et al., 2001, 2002; Victor et al., 2011): cortical pyramidal neurons (E), cortical inhibitory neurons (I), thalamo-cortical relay neurons (S), and thalamic reticular neurons (R). The

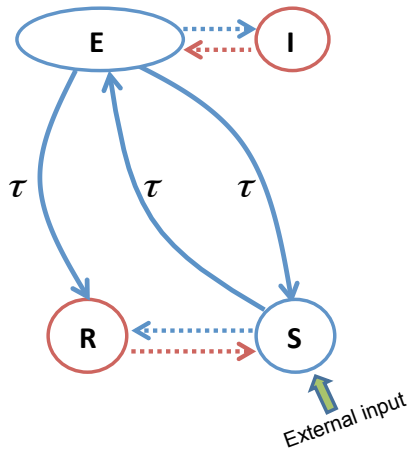


**Figure 1.** Schematic of a thalamo-cortical module. The blue arrows indicate excitatory connections and the red arrows represent inhibitory connections. The solid lines indicate connections associated with a same delay and the dotted lines represent connections without delay.

thalamo-cortical relay neurons receive input from, and project onto the cortical pyramidal neurons. They also project onto the thalamic reticular neurons. The cortical inhibitory neurons inhibit pyramidal neurons and receive excitatory input from them. The thalamic reticular neurons inhibit the thalamo-cortical relay neurons, and receive excitatory input from the pyramidal neurons. The excitatory connections between cortex and thalamus are associated with a conduction delay while no delay is present in the projections within the thalamus and within the cortex (Victor et al., 2011).

The underlying neural mass model considers an ensemble of neurons on a mesoscopic scale which includes two types of neurons, namely excitatory and inhibitory cells (Hutt and Longtin, 2009). The connection elements between neurons are excitatory and inhibitory chemical synapses in which both types of synapses may occur on dendritic branches of both cell types. The present model considers AMPA/NMDA and $GABA_A$ synaptic receptors. The model assumes spatially extended populations of both neuron types, which exhibit spatially synchronous population activity. This spatial synchronization represents a reasonable approximation to describe EEG-spectra measured on the scalp (Robinson et al., 2001).

Mean excitatory and inhibitory postsynaptic potentials $V^e(t)$ and $V^i(t)$ at time

$t$ obey the convolution

$$V^{e,i}(t) = \int_{-\infty}^{t} h_{e,i}(t-t')P_{e,i}(t')dt', \tag{1}$$

where $P_e(t)$ and $P_i(t)$ represent the mean presynaptic population firing rates which terminate at excitatory and inhibitory synapses, respectively. The functions $h_e(t)$ and $h_i(t)$ indicate the synaptic response function of excitatory and inhibitory synapses. In a reasonable approximation we assume an instantaneous rise of the synaptic response function followed by an exponential decay as

$$h_e(t) = a_e \alpha e^{-\alpha t} \quad , \quad h_i(t) = a_i f(p) \beta e^{-\beta t}, \tag{2}$$

where $1/\alpha$ and $1/\beta$ are the decay times of the response function for excitatory and inhibitory synapses, respectively. The function $f(p)$ reflects the action of propofol on the GABAergic synaptic receptors and is proportional to the charge transfer in these receptors. It will be estimated in the following subsection. Here the parameters $a_e$ and $a_i$ denote the synaptic gain which are taken as $1mVs$.

For convenience, the integral equations (1) may be formulated as differential equations

$$\hat{L}_e V^e(t) = a_e P_e(t) \quad , \quad \hat{L}_i V^i(t) = a_i f(p) P_i(t), \tag{3}$$

with $\hat{L}_e(\partial/\partial t) = \partial/\partial \alpha t + 1$, $\hat{L}_i(\partial/\partial t) = \partial/\partial \beta t + 1$. External input to the system originates from other neural populations and is considered as a non-specific input to relay neurons as

$$I(t) = I_0 + \xi(t), \tag{4}$$

where $I_0$ indicates its mean value and $\xi(t)$ is global Gaussian uncorrelated noise with

$$\langle \xi(t) \rangle = 0, \quad \langle \xi(t)\xi(t') \rangle = 2\kappa\delta(t-t'), \tag{5}$$

where $\langle . \rangle$ denotes the ensemble average and $\kappa$ is the intensity of the driving noise.

Moreover, the population firing rates $P_{e,i}$ in Eqs. (1) depend on the effective membrane potential in the corresponding populations. The present study considers a recently derived transfer function of a population of type I-neurons (Hutt and Buhry, 2014)

$$S_{(j)}(V) = Sig_{(j)}(V,0) - Sig_{(j)}(V,\gamma), \tag{6}$$

with

$$Sig_{(j)}(V,\gamma) = \frac{S_{max(j)}}{2}\left(1 + \mathrm{erf}\left(\frac{V - V_{th(j)} - \gamma\sigma^2}{\sqrt{2}\sigma}\right)\right) e^{-\gamma(V - V_{th(j)}) + \gamma^2\sigma^2/2}, \tag{7}$$

with $j \in \{C, T\}$, where $C$ and $T$ denote cortical and thalamic populations, respectively. The parameter $\gamma < \infty$ reflects the properties of type I-neurons whereas $\gamma \to \infty$ yields the standard formulation assuming McCulloch-Pitts neurons (Hutt, 2012) since $Sig_{(j)}(x, \gamma \to \infty) = 0$. The transfer function (6) also considers a distribution of firing thresholds of the neurons (Wilson and Cowan, 1973) and the more similar the firing thresholds in the neural populations, i.e., the smaller $\sigma$ and the larger $c$ leads to the steeper the sigmoidal function. The transfer function in Eq. (6) is not anti-symmetric to its inflection point anymore (Hutt, 2012) and exhibits a larger nonlinear gain (slope) for large potentials $V > V_{th}$ compared to small potentials $V < V_{th}$. This asymmetry results from the firing properties of type-I neurons, see (Hutt and Buhry, 2014; Hutt, 2012) for more details. We identify the population firing rates $P_{e,i}$ with the transfer function $S_{(j)}$.

*Effect of propofol on neural populations*

According to experimental results, it is now widely accepted that anesthetic agents act by binding directly to the specific protein targets (Chau, 2010). While it has been reported that many receptors and molecular targets contribute to general anaesthesia, there is a general agreement that $GABA_A$ receptors are important in mediating the inhibition during propofol administration (Zhou et al., 2012). It has been shown that propofol increases the decay time constant of $GABA_A$ synapses, and hence increases the total charge transfer in these synapses (Franks, 2008). Interestingly, although Kitamura et al. (2002) have illustrated that propofol has a negligible effect on the amplitude of synaptic response function in cortical neurons, it markedly increases amplitude, decay time, and thus charge transfer of $GABA_A$ inhibitory postsynaptic currents evoked in relay neurons in the thalamic ventrobasal complex (Ying and Goldstein, 2005a). Since $GABA_A$ receptors mediate most of the inhibitory synaptic transmission we have not included $GABA_B$ receptors in our model. The present model assumes that the inhibitory synaptic transmission within thalamus, i.e. from reticular neurons to thalamo-cortical relay cells, are mediated by $GABA_A$ receptors. Most previous theoretical studies have considered synaptic action in the cortex, whereas effects of anesthetics on synaptic $GABA_A$ receptors in the thalamus have been neglected. To investigate the possible importance of anesthetic action on thalamic inhibitory $GABA_A$ receptors, the present study considers anesthetic action in the thalamo-cortocal loops only - and does not look at drug actions within the cortex.

In order to mimic the experimental findings, we assume that increasing propofol concentration decreases the decay rate of the inhibitory synaptic response function, $\beta$ by $\beta = \beta^0/p$ with $p \geq 1$ (Steyn-Ross et al., 1999; Hindriks and van Putten,

2012; Hutt and Longtin, 2009), where $\beta^0$ denotes the inhibitory decay rate in the absence of propofol. The factor $p$ reflects the on-site concentration of propofol in the neural populations and $p = 1$ indicates the baseline condition. Increasing $p$ leads to a decrease in the decay time constant of inhibitory synapses and thereby an increase in the charge transfer in these synapses.

*Model equations*

In order to emphasize the essential role of the intra-thalamic inhibition for the generation of characteristic EEG pattern under anaesthesia sedation, we neglect inhibition within the cortex. This assumption simplifies the model under study, while later results shall reveal that the model is still adequate to reproduce observed changes in EEG rhythms within $\delta-$ and $\alpha-$activity bands.

The mean membrane potentials $V_a^c$ in the cortex ($a = E$), the thalamic population of relay ($a = S$) and reticular ($a = R$) neurons obey

$$\begin{aligned}
\hat{L}_e V_E^e(t) &= K_{ES} S_T[V_S^e(t-\tau) - V_S^i(t-\tau)], \\
\hat{L}_e V_S^e(t) &= K_{SE} S_C[V_E^e(t-\tau)] + I(t), \\
\hat{L}_i V_S^i(t) &= f(p) K_{SR} S_T[V_R^e(t)], \\
\hat{L}_e V_R^e(t) &= K_{RE} S_C[V_E^e(t-\tau)] + K_{RS} S_T[V_S^e(t) - V_S^i(t)],
\end{aligned} \tag{8}$$

evoked at excitatory ($c = e$) and inhibitory ($c = i$) synapses. Moreover $K_{ab}$ are the synaptic connection strengths in population $a$ originating from population $b$ and $\tau$ is the transmission time delay between cortex and thalamus. The somatic firing rate function (6) in the cortex $S_C[\cdot]$ is different to the thalamic firing rate function $S_T[\cdot]$, while it is identical for the relay and the reticular populations. The nominal parameter values for two sets of parameters are displayed in Table 1 in the absence of anesthetics.

*Theoretical power spectrum*

The Eqs. (8) obey the general delay system

$$\hat{\boldsymbol{L}}(p)\boldsymbol{X}(t) = \mathbf{f}(\boldsymbol{X}(t), \boldsymbol{X}(t-\tau), p) + \boldsymbol{I}(t), \tag{9}$$

with the activity variable vector $\boldsymbol{X}(t) = (V_E^e, V_S^e, V_S^i, V_R^e)$ and the nonlinear vector function $\mathbf{f} \in \mathbb{R}^4$ which includes the nonlinear transfer functions depends on the anesthetic factor $p$. The external input is written as $\boldsymbol{I}(t) = \boldsymbol{I}_0 + \boldsymbol{\xi}(t)$ with $\boldsymbol{I}_0 = (0, I_0, 0, 0)^\top$ and $\boldsymbol{\xi}(t) = (0, \xi(t), 0, 0)^\top$. The matrix operator $\hat{\boldsymbol{L}}(p) \in \mathbb{R}^{4\times4}$ includes all temporal operators $\hat{L}_{e,i}$ and depends on the anesthetic factor $p$.

**Table 1.** Model parameters, their symbols, and nominal values for two parameter sets

| Parameter | Symbol | Nominal value (set I, set II) |
|---|---|---|
| Maximum firing-rate of cortical population | $S_{max(C)}$ | (130, 200) Hz |
| Maximum firing-rate of thalamic population | $S_{max(T)}$ | (100, 210) Hz |
| Mean firing threshold of cortical population | $V_{th(C)}$ | (25, 10) mV |
| Mean firing threshold of thalamic population | $V_{th(T)}$ | (25, 15) mV |
| Firing rate variance | $\sigma$ | (10,12) mV |
| Type-I population effect constant | $\gamma$ | (0.05, 0.09) $\text{mV}^{-1}$ |
| Excitatory synaptic decay rate | $\alpha$ | (60,60) $s^{-1}$ |
| Inhibitory synaptic decay rate | $\beta$ | (10,50) $s^{-1}$ |
| Excitatory synaptic gain | $a_e$ | 1 mVs |
| Inhibitory synaptic gain | $a_i$ | 1 mVs |
| Synaptic strength from E to S neurons | $K_{SE}$ | (0.8, 0.2) mVs |
| Synaptic strength from E to R neurons | $K_{RE}$ | (0.2, 0.5) mVs |
| Synaptic strength from S to E neurons | $K_{ES}$ | (0.8, 2) mVs |
| Synaptic strength from S to R neurons | $K_{RS}$ | (0.1, 0.3) mVs |
| Synaptic strength from R to S neurons | $K_{SR}$ | (0.8, 0.1) mVs |
| Constant external input | $I_0$ | 0.1 mV |
| Intensity of external thalamic noise | $\kappa$ | 0.5 mV |
| Transmission delay between cortex and thalamus | $\tau$ | 40 ms |

Neglecting the random fluctuations $\xi(t)$ for the moment, then the resting state $\boldsymbol{X}_0 \in \mathbb{R}^4$, i.e. for which $\hat{\boldsymbol{L}} = \mathbf{1}$, is given by

$$\boldsymbol{X}_0 = \mathbf{f}(\boldsymbol{X}_0, \boldsymbol{X}_0, p) + \boldsymbol{I}_0. \tag{10}$$

We observe that the resting state depends on $p$ and hence on the anesthetic concentration. The current model follows the standard assumption Nunez and Srinivasan (2006); Robinson et al. (2001); David and Friston (2003); David et al. (2006) that the electric dipol generating the EEG is modeled well by fluctuations of the dendritic currents about the resting state. Hence small deviations from the resting state $\boldsymbol{Y}(t)$ generate the EEG and obey

$$\hat{\boldsymbol{L}}(p)\boldsymbol{Y}(t) = \boldsymbol{A}(p)\boldsymbol{Y}(t) + \boldsymbol{B}(p)\boldsymbol{Y}(t-\tau) + \boldsymbol{\xi}(t), \tag{11}$$

where $\boldsymbol{A}(p)$, $\boldsymbol{B}(p) \in \mathbb{R}^{4\times4}$ are constant matrices. In accordance to previous studies (Nunez and Srinivasan, 2006; Robinson et al., 2001; David and Friston, 2003), the EEG is generated by the population activity of pyramidal cortical cells $V_E^e$. Then the power spectrum of the EEG reads (Hutt, 2013)

$$P_E(\nu, p) = 2\kappa\sqrt{2\pi}\frac{R_N^2(\nu, p) + I_N^2(\nu, p)}{R_D^2(\nu, p) + I_D^2(\nu, p)}\,, \tag{12}$$

see the appendix for the definition of functions $R_N(\nu, p)$, $I_N(\nu, n)$, $R_D(\nu, p)$ and $I_D(\nu, p)$.

We point out that $R_N$, $I_N$ are proportional to the nonlinear gain $dS_T[V]/dV$ computed at the resting state of the system, while $R_D$, $I_D$ dependent on both nonlinear gains $dS_{T,C}[V]/dV$. Since the resting state depends strongly on the anesthetic concentration factor $p$, in turn the nonlinear gains computed at the resting state depends on $p$ as well.

*Spectral contributions*

The system fluctuations about the stationary state are a linear superposition of damped noisy oscillations whose frequencies are determined by the imaginary part of the characteristic roots of Eq. (11). To quantify the contribution of each root to the power spectrum, we select a certain root and consider the fluctuations $\boldsymbol{Y}(t) = [y_1(t), y_2(t), y_3(t), y_4(t)]^\top$ with $y_n(t) = \hat{u}_n e^{\lambda t} + \hat{u}_n^* e^{\lambda^* t}$, $n = 1, \ldots, 4$. Here $\lambda$ is the root and $\hat{u}_n$ is the n-th element of the corresponding eigenvector. Then for each root

$$w_n = \frac{\int_0^{2\pi} y_n^2(t)dt}{w_1 + w_2 + w_3 + w_4}, \tag{13}$$

reflects the power in a certain oscillation mode with root $\lambda$. Since roots are associated to certain frequency bands, $w_n$ indicate the contribution of population $n$ to the power spectrum in a certain frequency band. Recall that $w_1$ is the contribution of excitatory currents in cortical neurons, $w_2$ reflects the contribution of the excitatory currents in the relay neurons, $w_3$ the contribution of inhibitory currents in relay neurons and $w_4$ the contribution of excitatory currents in reticular neurons.

To further illustrate the relative contribution of the sub-circuits $E \to S \to E$, $S \to R \to S$ and $E \to R \to S \to E$ (cf. Fig. 1) to the power in certain frequency bands, we define the relative frequency response function from neurons of type $b$ to neurons of type $a$

$$\eta_l(\nu, p) = \frac{|\chi_l(\nu, p)| - |\chi_l(\nu, p = 1)|}{|\chi_l(\nu, p = 1)|}, \tag{14}$$

where $l \in \{ese, srs, esre\}$, $\chi_{ese} = \xi^e_{es}\xi^e_{se}$, $\chi_{srs} = \xi^i_{sr}\xi^e_{rs}$ and $\chi_{esre} = \xi^e_{es}\xi^i_{sr}\xi^e_{re}$ and

$$\xi^{e,i}_{ab}(\nu, p) = K_{ab} S'_{C,T}(V^{*e,i}_b)\phi^{e,i}(\nu, p)e^{-2\pi i\nu\tau} \ . \tag{15}$$

The relative frequency response function $\eta_l$ is motivated by a similar measure defined by Hindriks and van Putten (2012) but extends this previous definition by its frequency dependence. Here $S'_{C,T}(V^{*e,i}_b)$ are the nonlinear gains, i.e. the derivative of the somatic firing function with respect to the voltages $V^{e,i}_b$ computed at the stationary states $V^{*e,i}_b$. The term $e^{-2\pi i\nu\tau}$ denotes the phase shift due to the propagation delay between cortex and thalamus for the pair of $(a, b) \in \{(e, s), (s, e), (r, e)\}$, and since it does not reflect any changes in our results, can be neglected in the analysis. The functions $\phi^{e,i}$ are the Fourier transform of $h_{e,i}(t)$ and represent the synaptic frequency responses

$$\phi^e(\nu, p) = 1/(1 + 2\pi i\nu/\alpha) \quad , \quad \phi^i(\nu, p) = f(p)/(1 + 2\pi i\nu/\beta(p)). \tag{16}$$

Increasing the factor $p$ decreases the decay rate of synaptic inhibition $\beta$ and increases the charge transfer $f(p)$. Hence the enhancement of inhibition leads to increased inhibitory synaptic frequency response function $\phi^i_{ab}$ given by Eq. (16). Moreover the administration of propofol changes the resting states and consequently the nonlinear gain functions $S'_{C,T}(V^{*e,i}_b)$ which may increase or decrease.

The $\delta-$ and $\alpha-$frequency bands are defined in the range [1Hz; 4Hz] and [8Hz; 12Hz], respectively.

## 3. Results

### *3.1. Experimental power spectrum*

An example of the time course of the progressive increase in propofol effect-site concentrations, and the changes in $\delta-$ and $\alpha-$power in each of the 11 para-midline electrodes are shown in Fig. 2(**A**) and (**B**), respectively. Figure 2(**C**) shows the full spectra averaged over frontal and occipital electrodes. The power spectra for frontal and occipital EEGs during the baseline phase and during sedation are shown in Fig. 2(**D**). They (see also Fig. 2(**E**)) show typical changes in EEG patterns; namely that the propofol resulted in a loss of the $\alpha-$rhythm (10 Hz) in the occipital electrodes, but a gain in $\alpha-$ and $\beta-$power (peak frequency around 13 Hz) in the frontal leads ($p < 0.05$, t-test). Propofol also causes an increase in $\delta-$power in both frontal and occipital regions ($p < 0.05$, t-test).
Figure 2(**D**) and (**E**) consider propofol concentrations which lead to sedation. In some patients, there is an increased activity in the frontal $\beta-$band which is seen at about 6 min in Fig. 2(**C**). The alternations in higher frequencies are not specifically investigated in our model.

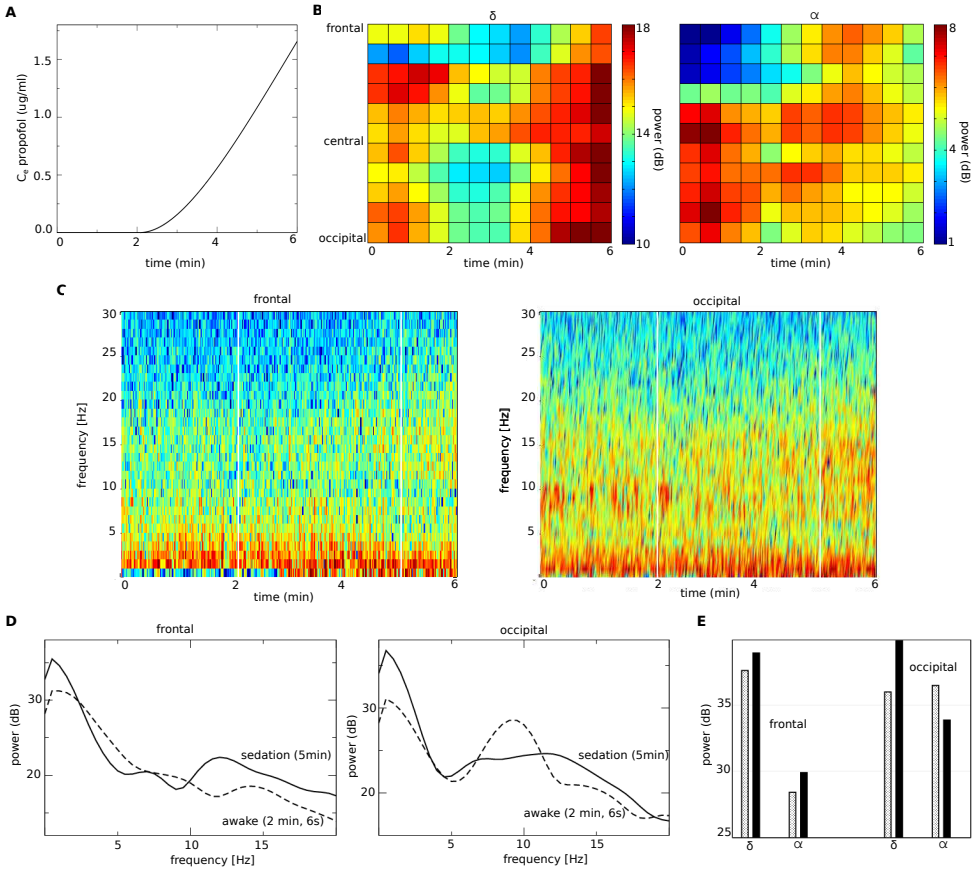


**Fig. 2.** Electroencephalographic data observed under anaesthesia sedation in a single subject while increasing the propofol concentration. (**A**) Blood plasma concentration of propofol with respect to administration time. (**B**) Mean spectral power in the $\delta-$ and $\alpha-$frequency bands in single electrodes located along the scalp mid-line with respect to administration time. (**C**) Spectrogram of power averaged over frontal and occipital electrodes. The vertical white lines denote 2 sec-time windows at 2 min 6 sec and at 5 min. (**D**) Power spectra averaged over four frontal (left) and four occipital (right) electrodes before the loss of consciousness (awake) and after the loss of consciousness (sleep). (**E**) Spectral power averaged over the $\delta-$ and $\alpha-$frequency bands in the frontal and occipital scalp. Grey and black color encodes awake and sedation.

### *3.2. Model power spectrum*

#### *3.2.1. Frontal spectrum*

Figure 3 shows the EEG power spectrum (12) in the baseline condition (absence of propofol) and after the administration of propofol for certain parameters (parameter set I in Table 1). We observe an increase of power in the $\delta-$ and $\alpha-$frequency bands while increasing the propofol concentration accompanied by $\alpha-$activity shifted to higher frequencies. These amplitude power changes bear a strong resemblance to the empirical observations in EEG power spectrum over the frontal region (cf. Fig. 3(**B**)). These results are confirmed by numerical simulations of the model.

To reveal the origin of the spectral EEG-changes with increasing concentration, we relate the maxima of spectral power to the roots of the characteristic equation of Eq. (11) $\lambda = \gamma + 2\pi i\nu$. Figure 4 shows the damping rate $\gamma$ and frequency $\nu$ of the roots in the $\delta-$ and $\alpha-$frequency ranges. Whereas the power peak in $\alpha-$frequency increases by the administration of propofol, the $\delta-$frequency is maintained for different propofol concentrations. Moreover, the damping rate of $\delta-$ and $\alpha-$activity increase with increasing anaesthetic level and hence the power in the corresponding frequency band increase after standard spectral theory.

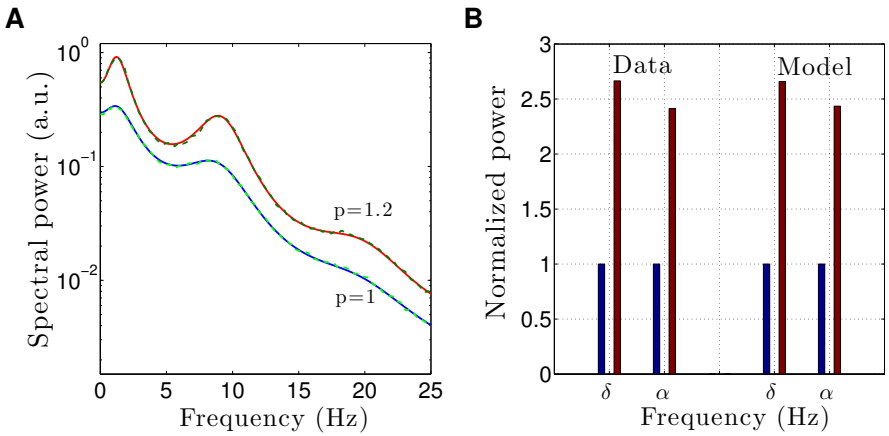


**Fig. 3.** The theoretical and experimental EEG-spectral power in the baseline and the anaesthesia sedation condition. (**A**) The solid lines indicate the analytical solutions and the dashed lines show the numerical solutions of the model system for the control condition ($p = 1$) and under sedation ($p = 1.25$). (**B**) The normalized power amplitude of experimental data in frontal electrodes and the model over $\delta-$ and $\alpha-$band in the baseline condition (blue bars) and in the anaesthesia sedation condition (red bars). Parameters are taken from set I in Table 1, the spectrum is computed at the higher stationary state of the system.

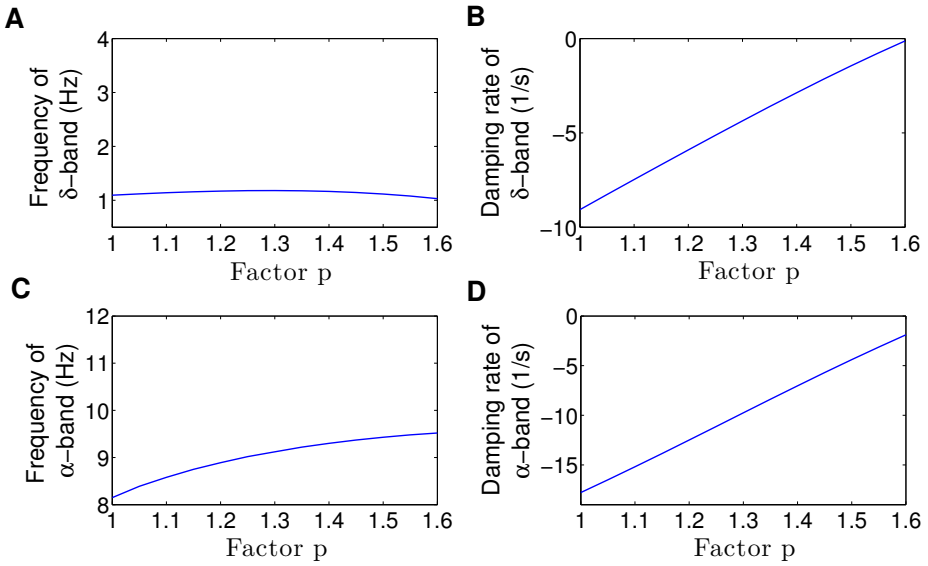


**Fig. 4.** Modulation of $\delta-$ and $\alpha-$activity resembling the dynamics over the frontal EEG-region. The panels show the frequency $\nu$ in the root's imaginary part which lie in the $\delta-$and $\alpha-$frequency ranges in panels (**A**) and (**C**), respectively and the corresponding damping rates in (**B**) and (**D**), respectively as a function of the anaesthetic factor $p$.

*3.2.2. Occipital spectrum*

For different parameters (set II in Table 1), Fig. 5 shows the model power spectrum resembling experimental activity observed in occipital EEG-electrodes. The power in the $\delta-$ frequency range increases and the $\alpha-$power decreases while increasing the anaesthetic level (cf. Fig. 5(**B**)). Figure 6 presents the effect of increasing propofol concentration on damping rate and frequency of the model EEG in the $\delta-$ and $\alpha-$frequency ranges. It can be observed that as propofol concentration increases, the damping rate of $\delta-$activity increases whereas $\alpha-$damping rate decreases. This finding is consistent with enhanced $\delta-$ and attenuated $\alpha-$power observed experimentally. In addition, the frequency of the activity in both frequency bands increase very slightly.

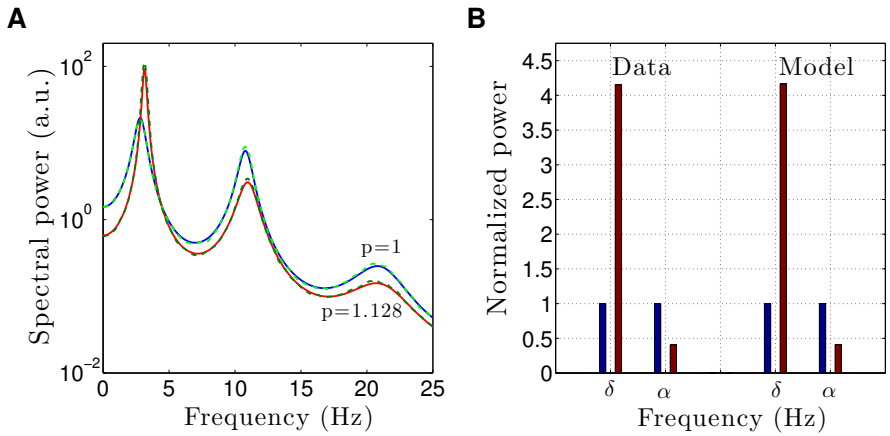


**Fig. 5.** EEG-spectral power compared to the power observed experimentally in occipital EEG-electrodes in baseline and under sedation. (**A**) The solid and dashed lines indicate the analytical and numerical solutions, respectively, in the baseline ($p = 1$) and in the anaesthesia sedation condition ($p = 1.128$). (**B**) The blue and red bars show the normalized power amplitude in the baseline and anaesthetic condition, respectively. Parameters are taken from set II in Table 1, the spectrum is computed at the lower stationary state of the system.

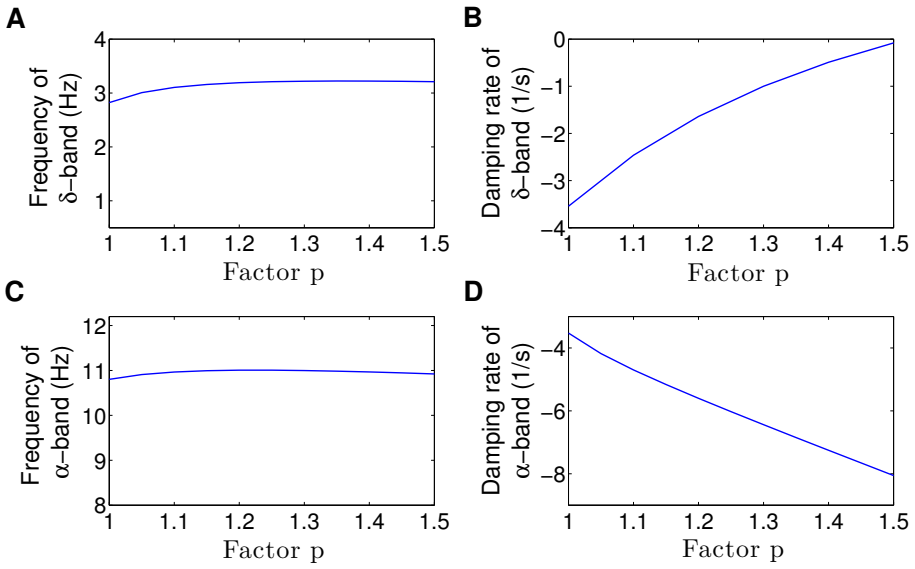


**Fig. 6.** Modulation of $\delta-$ and $\alpha-$activity over occipital region. Shown are the frequency of $\delta-$and $\alpha-$oscillation in (**A**) and (**C**), respectively and the corresponding damping rates in (**B**) and (**D**), respectively as a function of the factor $p$.

### *3.3. Resting state and gain function*

Figure 7 presents the mean potential of pyramidal neurons $V_E^{*e}$ in the resting state and the corresponding nonlinear gain dependent on the propofol concentration for the two parameter sets considered in the previous section. We observe that three resting states may occur in the baseline condition, cf. Fig. 7(**A**) and (**B**). Moreover, the upper and the center resting states collide at a critical value of $p$. Above this critical level, there exists a single resting state only at a low membrane potential. The stability study of the resting states reveal that the upper and lower resting states are linearly stable, whereas the center resting state is unstable. This shows that the system may evolve either about the upper or the lower state, but never about the center resting state.

Since the spectral power depends heavily on the resting state and the nonlinear gain, the distinction between the upper and lower resting states is important to understand the power changes shown in the previous section and in experiments. Increasing the anaesthetic concentration decreases the potential of the upper resting state and, since the upper membrane potential values are larger than the mean firing threshold and by virtue of the sigmoidal shape of the transfer function, decreasing $V_E^{*e}$ on the upper resting state leads to an increase of the corresponding nonlinear gain function (Fig. 7(**C**) and (**D**)). In contrast, increasing the anaesthetic level on the lower resting state decreases the nonlinear gain.

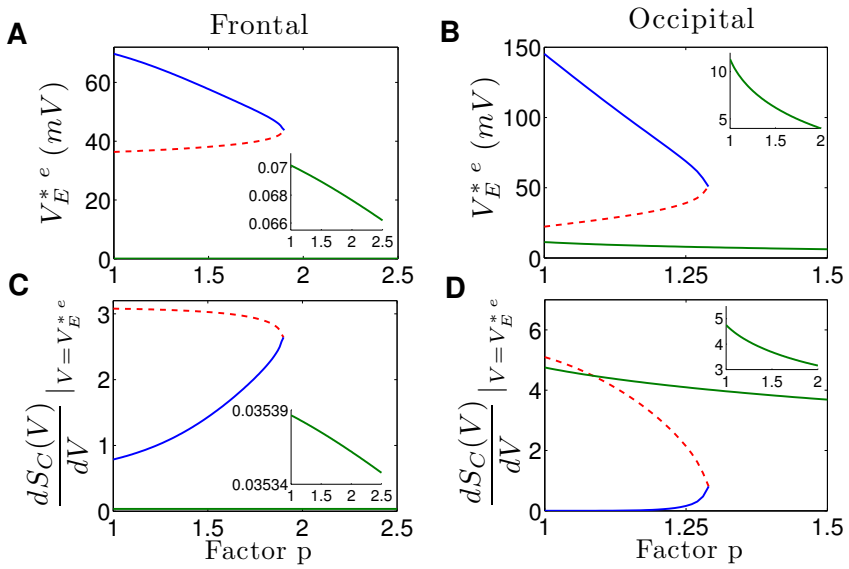


**Fig. 7.** The resting states of the system determined by Eq. (10) subject to the anaesthetic level. The panels (**A**) and (**B**) show values of $V_E^{*e}$ in the resting states for the two parameter sets I and II, respectively. Panels (**C**) and (**D**) present the corresponding nonlinear gain function $dS_C/dV$. The upper and lower stable branches are displayed respectively in solid blue and green lines whereas the middle unstable branches are encoded in dashed red lines. For illustration reasons, the lower branches are shown again in the insets.

### 3.4. Role of different populations

#### 3.4.1. Frontal spectrum

In order to understand the role of different populations of the employed thalamocortical module, we study the power spectra and their contributions in the different brain areas. Taking a closer look at the origin of the frontal EEG, Fig. 8(**A**) shows the spectral power of the system fluctuating about the upper stationary state. Panels (**B**) and (**C**) give the relative contribution $\{w_n\}$ of the respective populations in the $\delta-$ and $\alpha-$frequency bands, respectively. Under light sedation, the spectral power is well enhanced within the $\delta-$ and $\alpha-$band in comparison to the baseline condition. As seen in Fig. 8(**B**) and (**C**), the cortico-thalamic relay loop *ese* ($V_E^e$ and $V_S^e$) contribute most to the $\alpha-$activity while the thalamic populations generate the activity in the $\delta-$band (PSPs $V_S^i$ and $V_S^e$).

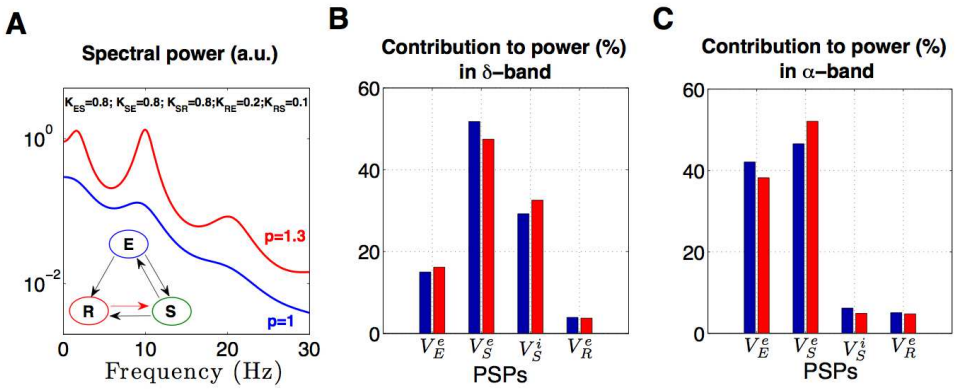


**Fig. 8.** The spectral power and the partial contributions in the brain areas describing activity in the frontal electrodes. (**A**) power spectrum in the baseline ($p = 1$, blue) and sedation condition ($p = 1.3$, red). (**B**) Contributions $w_n$ (cf. Eq. (13)) in $\delta-$band and (**C**) the $\alpha-$band. The system fluctuates about the upper resting state of the system. Parameters are $\beta_e = 70, \beta_i = 40$, and others are taken from set I in Table 1.

#### 3.4.2. Occipital spectrum

To investigate the occipital EEG in some more detail, we consider different topological configurations in the module to study $\delta-$ and $\alpha-$activity. Figure 9 shows the power spectra and the relative contribution $\{w_n\}$, generated by different

anatomical loop configurations computed at the lower resting state of the system in the baseline and anaesthetic conditions. At first, the plots reveal that the anaesthetic state always exhibits a diminished $\alpha-$power compared to the baseline condition, while the effect on the $\delta-$activity depends strongly on the configuration. The simplest topology (I) includes a reciprocal projection between cortical pyramidal neurons (E) and thalamo-cortical relay neurons (S) associated with a time delay (*ese* loop). This cortico-thalamic relay loop generates $\alpha-$activity with a power spectral peak at about 10 Hz. The loop also generates activity in the $\delta-$band but no power spectral peak at about 4 Hz as observed in Fig. 5. Figure 9(**B**) and (**C**) reveal that this loop contributes to both the $\delta-$ and $\alpha-$power. Since no inhibitory synapses are involved, the spectrum is independent of the anaesthetic level.

Adding the additional thalamic loop between relay and reticular neurons to the *ese* loop (as seen in (II)) retains the $\alpha-$power peak and still does not generate a spectral peak in the $\delta-$band. The cortical and thalamo-cortical relay populations contribute most to both frequency bands as seen in Fig. 9(**B**) and (**C**).

Configurations (I) and (II) in Fig. 9 do not exhibit the cortico-thalamic closed loop as found in physiology since the cortico-reticular connection is missing. Adding this connection to a reticular-relay and a relay-cortical connection, the system exhibits strong oscillations at about 4 Hz with a clear corresponding spectral peak. This peak occurs for the simple closed loop shown in configuration (III) but neglects the thalamic feedback and the cortico-relay connection. This configuration exhibits a disrupted cortico-thalamic relay loop which yields the loss of the prominent $\alpha-$peak as seen in Fig. 9(**A**). Figure 9(**B**) and (**C**) show clearly that primarily the thalamic populations generate the activity in the $\delta-$ and $\alpha-$band.

For the full configurations (IV) and (V), the power spectra always exhibit an $\alpha-$ and $\delta-$peak. Only configuration (V) induces stronger $\delta-$activity under anaesthetic condition than in baseline condition, while configuration (IV) exhibits less activity in the anaesthetic condition than in the baseline condition. The difference in the spectral properties between (IV) and (V) results from a stronger relay-cortical connection. As seen in Fig. 9(**B**) and (**C**), the excitatory synaptic currents in the reticular and cortical population (proportional to $V_R^e$ and $V_E^e$, respectively) contribute most to the $\alpha-$activity while the $\delta-$activity is primarily generated in the thalamic areas ($V_R^e$ and $V_S^i$).

To further reveal the role of cortico-reticular, reticular-relay and relay-cortical connections (*esre* loop in Fig. 9(III)) in the generation of the $\delta-$activity, we investigate the effect of connection strengths in this loop on the imaginary part (frequency) and real part (damping rate) of the characteristic root corresponding to the

$\delta-$activity. Figure 10 illustrates that the frequency and the damping rate increase with increasing the cortico-reticular, reticular-relay and relay-cortical connections indicating an increase of frequency and magnitude in the $\delta-$band. An additional study (not shown) of the remaining connections, i.e. from relay to reticular cells and from cortical to relay cells, reveals a negligible change of the $\delta-$power. These results suggest a major contribution of the *esre* loop to the $\delta-$activity in the system.

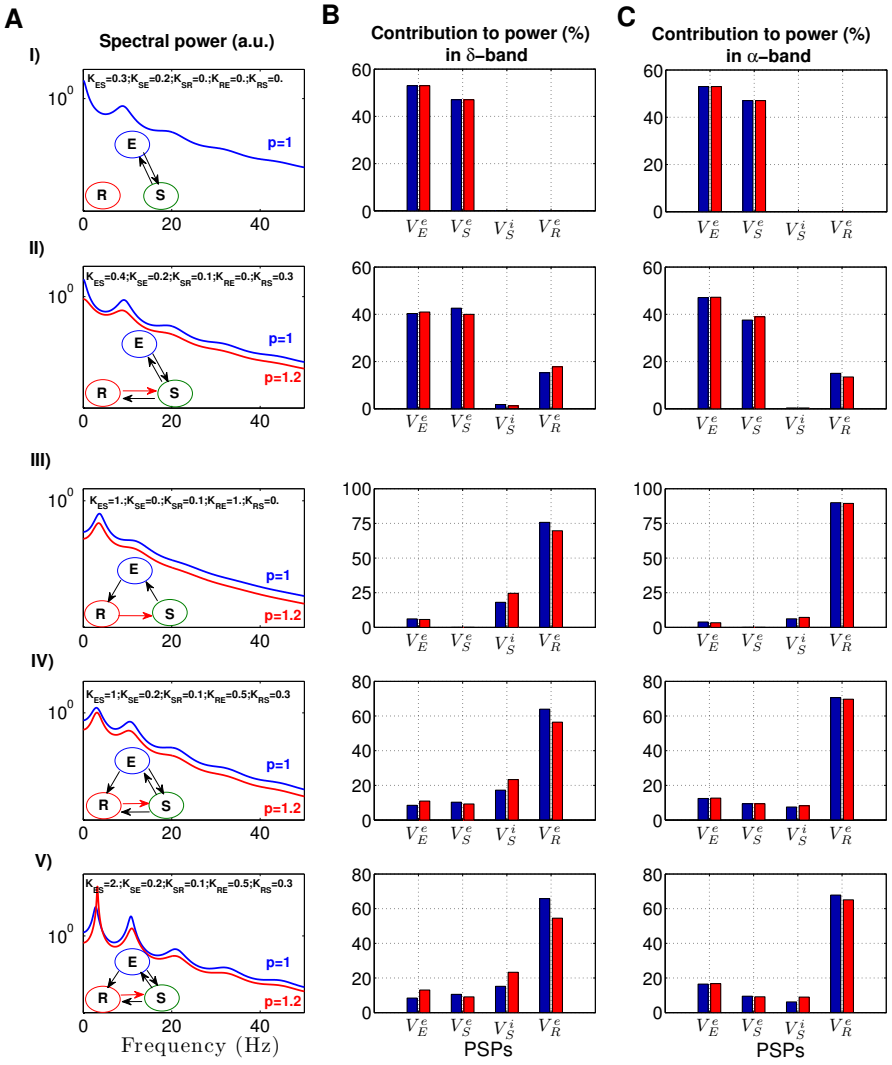


**Fig. 9.** Different topological configurations, their resulting spectral power in the baseline condition ($p = 1$, blue) and anaesthesia sedation ($p = 1.2$, red) (**A**) and the contributions to power $w_n$ (cf. Eq. (13)) in $\delta-$band (**B**) and $\alpha-$band (**C**), respectively. The systems fluctuates about the lower resting state of the system and parameters are taken from set II in Table 1.

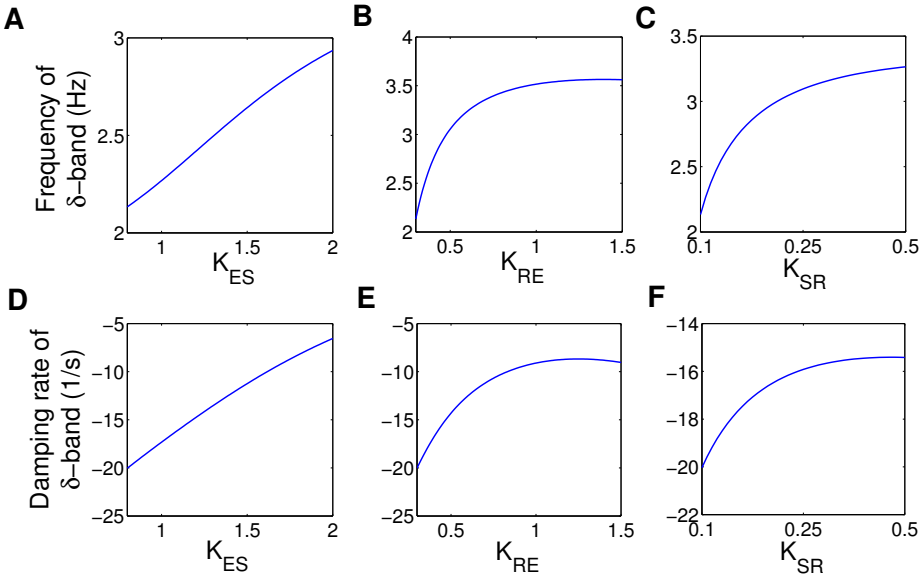


**Fig. 10.** Modulation of the frequency and corresponding damping rate of the $\delta-$activity by increase in the coupling strengths $K_{ES}$ in (**A**,**D**), $K_{RE}$ in (**B**,**E**) and $K_{SR}$ in (**C**,**F**). Parameters are $K_{ES} = 0.8$, $K_{RE} = 0.3$, $K_{SR} = 0.1$, $K_{SE} = 0.1$, $K_{RS} = 0.2$, and others are taken from set II in Table 1.

### 3.5. Sub-circuits

Figure 11 illustrates the contribution of three different anatomical loops $l \in \{ese, srs, esre\}$ to the power spectrum at the upper and lower resting states of the system corresponding to the frontal and occipital regions respectively.

In the upper resting state, increasing the propofol concentration increases the inhibitory synaptic frequency response function $\phi^i_{ab}$ (cf. Eq. (16)) as well as the nonlinear gain functions $S'_{C,T}(V_b^{*e,i})$ (cf. Fig. 7(**C**)). Hence, as observed in Fig. 11(**A**), the relative frequency response function $\eta_l$ in the $\delta-$ and $\alpha-$band increases for all loops. This affirms the enhancement of the power in $\delta-$ and $\alpha-$band observed over frontal electrodes.

At the lower resting state, increasing propofol concentrations increases the inhibitory synaptic frequency response function $\phi^i_{ab}$ but the nonlinear gain functions $S'_{C,T}(V_b^{*e,i})$ decrease (cf. Fig. 7(**D**)). As observed in Fig. 11(**B**), since no inhibitory synapses are involved in the $ese$ loop, $\eta_{ese}$ decreases with a decreasing nonlinear gain function. This reveals an important role for the $ese$ loop in the modulation of $\alpha-$activity which decreases by decreasing the gain function, in contrast to the upper resting state.

Within the $srs$ and $esre$ loops, the nonlinear gains at the lower resting state decrease by an increase of the propofol concentration while the increase in the inhibitory charge transfer more than compensates this decrease essentially leading to an increase in $\eta_{srs}$ and $\eta_{esre}$. Consequently the enhancement of inhibition plays a more substantial role than the gain function modulation.

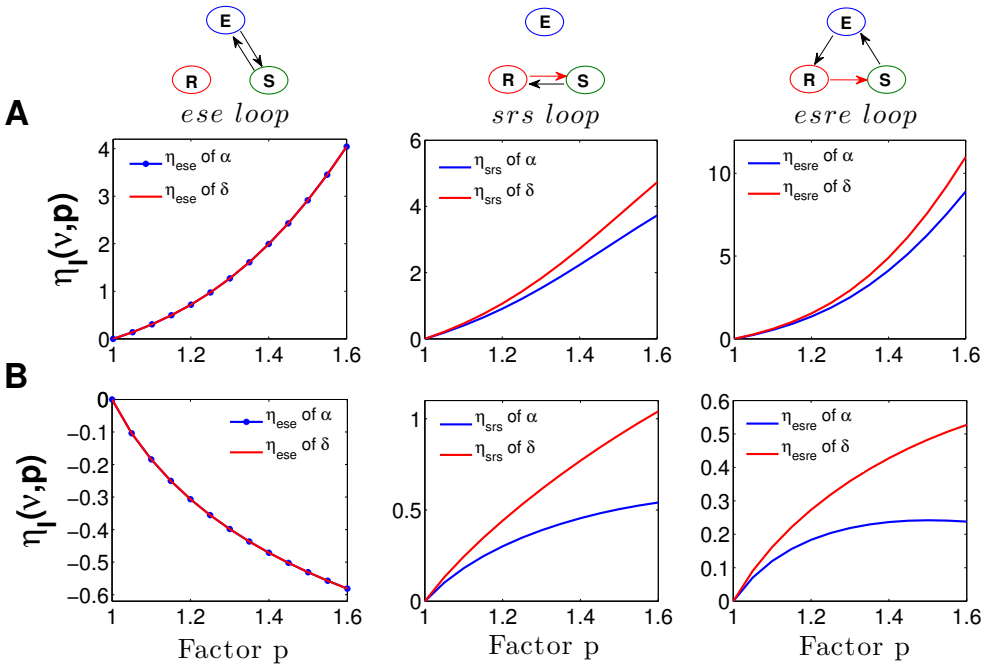


**Fig. 11.** The change of the relative frequency response function $\eta_l(\nu, p)$ defined by Eq. (14) in the $\delta-$ and $\alpha-$frequency bands within different anatomical loops of the thalamo-cortical system. The panels in (**A**) consider fluctuations about the upper resting state and panels in (**B**) give the results at the lower resting state.

### 3.6. *Full model*

Finally, to reveal the role of the cortical inhibitory neurons, we have studied in addition the thalamo-cortical module shown in Fig. 1 comprising the cortical inhibitory population in contrast to the previous studies. Figure 12 shows the power spectra of EEG over frontal and occipital regions in the baseline and in the anaesthetic conditions computed at the upper and lower stationary states of the system. It turns out that this extended models yields similar results compared to the reduced model (8), (cf. Figs. 3 and 5 ) neglecting cortical inhibition, i.e. one can either retain or neglect the cortical inhibitory population.

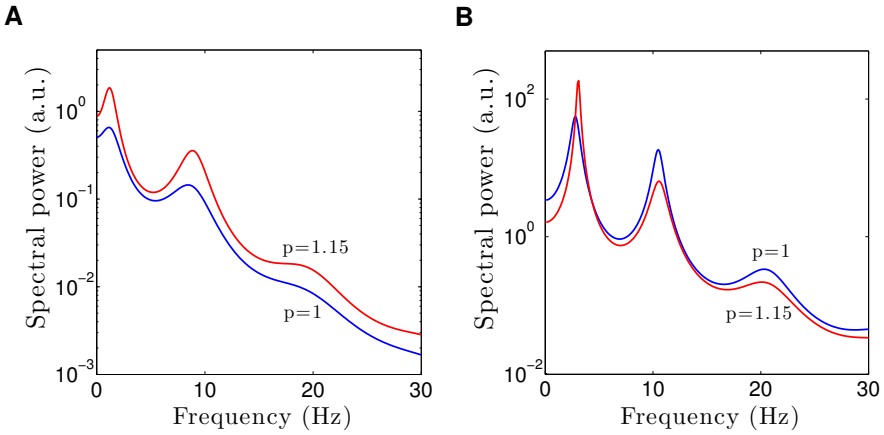


**Fig. 12.** The spectral power of EEG associated with the full thalamo-cortical module shown in Fig. 1, i.e. considering cortical inhibition, in the baseline condition ($p = 1$) and under sedation ($p > 1$). The panels show the spectrum over frontal region in (**A**) and over occipital region in (**B**) computed at the higher and lower stationary states of the system, respectively. Parameters in (**A**) are $K_{ES} = 0.8$, $K_{EI} = 0.6$, $K_{IE} = 0.2$, $K_{SE} = 0.8$, $K_{SR} = 0.8$, $K_{RE} = 0.2$, $K_{RS} = 0.1$, and in (**B**) $K_{ES} = 2.2$, $K_{EI} = 0.4$, $K_{IE} = 0.2$, $K_{SE} = 0.2$, $K_{SR} = 0.1$, $K_{RE} = 0.5$, $K_{RS} = 0.3$, $S_{max(C)} = 140$, $S_{max(T)} = 210$, $V_{th(C)} = V_{th(T)} = 10$, the additional excitatory and inhibitory decay rate is $\alpha = 50$ and $\beta = 40$, respectively. Others parameters are taken from sets I, II in Table 1.

## 4. Discussion

### *4.1. Origin of spectral peaks*

A large class of general anaesthetics such as propofol act on inhibitory GABAergic synaptic receptors and hence enhance the inhibition in the neural populations. Accordingly one might expect that the stronger inhibition caused by propofol would reduce spectral power. The opposite is the case; stronger inhibition induces a power surge in certain frequency bands. Figures 4 and 6 explain this power surge by propofol-induced approach of the system dynamics to dynamical oscillatory instabilities. In the control condition the external random fluctuations from other cortical and non-cortical areas are well damped except for the $\alpha-$frequency band. The power surge of $\alpha-$activity indicates that the system is lying in the vicinity of an oscillatory instability point. This explanation follows previous ideas about the origin of $\alpha-$activity (Robinson et al., 2001; Drover et al., 2010; Hindriks and van Putten, 2012; Hutt, 2013). If the system is lying on the upper resting state, increasing the synaptic inhibition by increasing the anaesthetic concentration moves the system closer to the instability point, decreases the damping of external fluctuations and hence may lead to an increase of power as observed in Fig. 3 for frontal electrodes. In contrast, if the system is lying on the lower branch increased inhibition moves the system away from the oscillatory instability point what yields a decrease of power as observed in occipital electrodes, cf. Fig. 5.

To explain the origin of the power surge in the $\delta-$frequency band, a slightly different mechanism comes into play since no spectral peak in the $\delta-$range is present in the control condition. Hence increased synaptic inhibition may not only move the system towards an already existing instability point, but actually also generates this instability point for increased inhibition. Figures 4 and 6 explain the origin of the power surge in the $\delta-$frequency band by the generation of an oscillatory instability at frequencies in the $\delta-$band. A more detailed analysis (cf. Fig 8) reveals that the $\delta-$power surge is initiated at values $p > 1$, i.e., does not occur in the control condition ($p = 1$) but for increased anaesthetic concentration only. Hence, the spectral power peak in the $\delta-$frequency band originates from the propofol-induced inhibition.

Our model results both extend and contrast previous findings. The model is one of the first taking into account the explicit anaesthetic action of propofol on thalamic GABAergic synaptic receptors, cf. Fig 2. The model explains both the changes in the EEG in the $\delta-$ and the $\alpha-$frequency bands and describes well the anteriorization of both the $\alpha-$ and $\delta-$rhythms, i.e., the distinct dynamics in both frontal and occipital cortical regions.

Nevertheless, to investigate the importance of cortical inhibition, Fig. 12 shows clearly that additional cortical inhibition might yield similar results. Consequently, it is not necessary to consider cortical inhibition to describe the experimental power spectrum under sedation. This result contrasts the finding of Hindriks and van Putten (2012) who point out the importance of intra-cortical inhibition. The neglect of cortical inhibition reduces the dimensionality of the model as well as put emphasis on the effect of propofol on the inhibitory synaptic receptors in the thalamic cells.

This result shows that it is possible to replicate many observed EEG phenomena by modelling anaesthetic action on purely the thalamo-cortical loops. Several previous studies explaining EEG by a cortico-thalamic model consider both thalamic and cortical anaesthetic action (Hindriks and van Putten, 2012; Ching et al., 2010; Vijayan et al., 2013; McCarthy et al., 2008) and point out the importance of cortical anaesthetic action. Even pure cortical models (Liley and Bojak, 2005; Wilson et al., 2006) may explain several spectral features observed in EEG under anaesthesia. Most of these previous models are either rather complex with several tens of free parameters and hence many degrees of freedom permitting to fit the experimental data for a small subset of parameters (Liley and Bojak, 2005; Wilson et al., 2006) or identify specific single neuron mechanisms to be responsible for a certain anaesthetic effect in macroscopic EEG, e.g. as in Ching et al. (2010); Vijayan et al. (2013); McCarthy et al. (2008). In contrast, our model is comparatively simple while elucidating the major underlying mechanism: the activation of pre-defined oscillation modes whose amplitude and frequency depends on the level of synaptic inhibition.

The present work considers light sedation, i.e., low propofol concentrations, far from those required for full surgical anaesthesia. Some previous studies have investigated in detail the EEG power spectra at higher concentrations of propofol where additional characteristic features emerge, such as burst suppression (Ching et al., 2010, 2012), broad spatial EEG coherence (Cimenser et al., 2011; Murphy et al., 2011; Gugino et al., 2001; Purdon et al., 2012), strong spectral power in the $\beta-$band (McCarthy et al., 2008; Purdon et al., 2012) and functional fragmentation accompanied by a drop of population firing rate and increased spectral power at frequencies $< 1$ Hz (Lewis et al., 2012). For instance, Fig. 2(C) shows emerging $\beta-$activity well after light sedation that we consider in the present work. Our model does not explain these latter features, since they emerge for higher propofol concentrations and may result from fundamental changes in the interaction

between neural structures, cf. (Ching et al., 2010) explaining the $\beta-$power surge by the interaction of two thalamo-cortical modules.

Our reduced model describes very well the action of propofol on neural populations in the cortex and thalamus while the fundamental interactions of cortex, thalamus and other sub-cortical structures such as the brainstem and hippocampus are retained. In contrast, larger concentrations affect not only the activity in single populations but also the interaction between a larger set of neural structures. This strong effect on the inter-area interactions has been been quantified in several previous experimental studies and has been termed fragmentation or connectivity break-down (Lewis et al., 2012; Boly et al., 2012; Massimini et al., 2005).

### *4.2. Multiple resting states*

Experimental EEG under propofol anaesthesia shows an anteriorization in the $\delta-$ and $\alpha-$frequency bands (Purdon et al., 2012; Cimenser et al., 2011; Lewis et al., 2012). The recent study of Vijayan et al. (2013) is one of the first to explain the distinct evolution of spectral power. They suggest two distinct models for the anteriorization during propofol anaesthesia: one for the frontal and one for the occipital EEG $\alpha-$activity, where the occipital cortico-thalamic connection exhibits an additional hyperpolarizing mechanism lowering the resting state population firing rate. At a first glance, this description is similar to our model explaining the anteriorization by the existence of high- and low-activity resting states. However, our model extends the explanation of Vijayan et al. (2013) by providing a model for both the $\delta-$ and the $\alpha-$frequency bands and explain the effect by the nonlinear gain functions in the corresponding resting states. Our mathematical analysis of the power spectrum (12) reveals that only increasing nonlinear cortical gain functions induce a power surge in the $\alpha-$range whereas decreasing nonlinear cortical gain functions diminish the $\alpha-$power. Since increases in the nonlinear gain occur at high activity-resting states only while decreasing nonlinear gains are present in low activity-resting states (Fig. 7), our findings suggest the important role of multiple resting states at high and low population firing rates and affirms previous EEG modelling studies Victor et al. (2011); Drover et al. (2010); Steyn-Ross et al. (2001b) pointing out the importance of multiple resting states to explain resting state EEG. In contrast, the evolution of the $\delta-$power is rather independent of the resting state and increases for increasing propofol concentrations for both increasing and decreasing nonlinear gains. Summarising, the $\alpha-$rhythm is fundamentally different from the $\delta-$rhythm.

*4.3. Effective sub-circuits in the cortico-thalamic module*

The origin of $\delta-$rhythm appears to be fundamentally different to the origin of $\alpha-$rhythm. A detailed analysis of the spectral contributions of the populations to $\delta-$ and $\alpha-$power, cf. Figs. 9 and 8, reveals that strong $\delta-$power occurs primarily when there is a strong connection between thalamic areas (frontal spectrum) and from cortex to the reticular nucleus, reticular to relay nucleus and relay to cortex (*esre* loop for the occipital spectrum). Strong $\alpha-$power is generated primarily by the cortico-thalamic relay circuit (*ese* loop).

Having identified these sub-circuits, their subsequent detailed analysis reveals that the frontal enhancement and occipital attenuation of $\alpha-$activity originate primarily from a (frontal) increase and (occipital)decrease in the nonlinear gain function within the thalamo-cortical *ese* loops. In turn, this result supports the presence of multiple resting states derived in the earlier part of our analysis. Hence, we suggest that the phenomenon of anteriorization of $\alpha-$power results from fronto-occipital differences in the nonlinear gain functions in the cortico-thalamic relay circuits. The previous study of Vijayan et al. (2013) on the anteriorization of $\alpha-$activity supports a similar idea. These results are also in agreement with the recent findings of Hindriks and van Putten (2013). They show that changes of transfer function properties and synaptic parameters, directly or indirectly, lead to changes in the gain functions by altering the values of the resting states of the system that cause the $\alpha-$ response modulations. Their results affirm our hypothesis that the increase or decrease of $\alpha-$power spectrum depends profoundly on the the resting state values of the system and the corresponding nonlinear gain functions. This finding is well in line with previous modelling studies on the origin of occipital $\alpha-$activity in the absence of anaesthesia explaining the amplitude modification by modified nonlinear gain changes.

The changes in the $\delta-$frequency band are explained by increases in the charge transfer within the thalamic populations what results to an increase of the frequency response function within the *srs* and *esre* loops, which essentially enhances the $\delta-$power. This hypothesis on the interplay of nonlinear gain and synaptic inhibition has been briefly mentioned in a previous work (Hutt, 2013).

Our analysis aims to extract general interaction mechanism for the generation of spectral EEG characteristics. To this end, we employ a reductionist approach: starting from a simple model and extending it step by step to find a neurophysiologically reasonable minimal model that explains as much experimental features as possible. The approach is motivated by the insight that general anaesthesia

is a macroscopic global and fundamental effect that emerges in various different species although they exhibit different detailed neural structures. Consequently, the underlying mechanism should be rather unspecific in biological detail but rather general in concept. We have identified elements of principal underlying mechanisms to explain $\delta-$ and $\alpha-$power observed during propofol anaesthesia sedation, namely the nonlinear population gain, the level of synaptic inhibition and the interaction of neural sub-circuits (or microcircuits). It appears that one of the most important properties of the sub-circuits is their ability to generate an oscillation. Since these elements promise to reflect underlying principles, they are rather independent of the choice of the anaesthetic agent and may generalize to the larger class of anaesthetic GABAergic (Garcia et al., 2010) or volatile drugs (Grasshoff et al., 2006).

Several previous modelling studies have explained the $\alpha-$rhythm by the delayed thalamo-cortical feedback (Robinson et al., 2004; Victor et al., 2011; Drover et al., 2010) or by a purely cortical model, cf. e.g. (Spiegler et al., 2010, 2011; Hutt, 2013; Hindriks and van Putten, 2012). On a first glance these two explanations appear exclusive. However, according to the previous discussion, the underlying principle put forward in the present work is not contradictory to cortical and thalamo-cortical circuits since both represent oscillating sub-circuits: previous cortical models include feedback loops of excitatory and inhibitory populations and most thalamo-cortical feedback models oscillate due to the involved delay known to facilitate oscillations. Consequently, the $\alpha-$rhythm may originates from a general class of oscillating circuits. This interpretation is supported by the experimental findings that the brain is highly adaptive and brain areas may take over tasks of other areas as seen under general anaesthesia (Lee et al., 2010), in sleep (Siegel, 2009) or after brain injury (Wieloch and Nikolich, 2006).

Similarly, various sources and mechanisms have been proposed for EEG $\delta-$activity. Previous experimental studies suggest a cortical origin of $\delta-$waves under anaesthesia (Murphy et al., 2011) and point out the importance of the cortico-thalamic feedback in the generation of $\delta-$waves in anaesthesia (Boly et al., 2012) and sleep (Steriade et al., 1993; Dang-Vu et al., 2008), while $\delta-$activity during sleep may also result from a connected network of thalamus, brainstem and different cortical areas (Maquet et al., 1997). Our model results point out the importance of the intra-thalamic feedback of reticular and relay populations as part of the thalamo-cortical feedback loop, which is in full line with the previous literature.

### *4.4. Model limitations*

The majority of the study assumes pure thalamic anaesthetic GABAergic action, although cortical GABAergic action has been reported. We argue that this reduction is reasonable since the reduced model describes the spectral EEG features very well and the addition of cortical inhibition does not lead any large improvement, cf. Fig. 12.

Our model is sufficient for low concentrations of propofol, whereas higher anaesthetic concentrations lead to additional spectral EEG features not captured by the current model, such as an increase in $\beta-$power just before loss of consciousness (Purdon et al., 2012) or burst suppression patterns after loss of consciousness (Ching et al., 2012; Liley and Walsh, 2013). To consider these effects, a future model will incorporate additional thalamo-cortical modules and nonlinear dynamics in thalamic populations.

Moreover, the model neglects additional, possibly important, anaesthetic effects such as the tonic inhibition induced at extra-synaptic GABAergic receptors (Farrant and Nusser, 2005; Hutt, 2012) which are very sensitive to anaesthetics (Orser, 2006) and are supposed to determine the global level of inhibition (Semyanov et al., 2004; Belelli et al., 2009). A recent work on the effect of extra-synaptic anaesthetic action on neural populations Hutt and Buhry (2014) has elucidated how to incorporate this effect in the model presented in this work. In addition, extra-synaptic receptors are found in several sub-cortical areas (Kullmann et al., 2005; Farrant and Nusser, 2005) indicating a strong effect on the reticular activating system (RAS) (Vanini and Baghdoyan, 2013). Hence, to understand better the inhibitory homeostatic mechanisms in anaesthesia, it will be necessary to include the RAS and its involved sub-cortical areas.

## 5. Conclusion

We would conclude that - using a reduced model of cortico-thalamic loops - it is possible to replicate the different frontal and occipital changes in the $\alpha-$ and $\delta-$rhythms in the EEG, caused by modest concentrations of propofol. The $\alpha-$rhythm is primarily dependent on the cortico-thalamic relay interaction, whereas the increased propofol reticular nucleus inhibition acting via the full thalamo-cortical loop are necessary for the increase in $\delta-$ waves. This model also offers a plausible explanation of the eyes-closed occipital alpha rhythm.

## 6. Acknowledgements

The authors acknowledge funding from the European Research Council for support under the European Union's Seventh Framework Programme (FP7/2007-2013)/ERC grant agreement no. 257253.

## Appendix A. Stationary states

The mean excitatory and inhibitory postsynaptic potentials in the cortical pyramidal neurons ($E$), cortical inhibitory neurons ($I$), thalamo-cortical relay neurons ($S$) and thalamic reticular neurons ($R$) shown in Fig. 1 obey

$$\begin{cases} \hat{L}_e V_E^e(t) = K_{ES} S_T[V_S^e(t-\tau) - V_S^i(t-\tau)], \\ \hat{L}_i V_E^i(t) = p K_{EI} S_C[V_I^e(t)], \\ \hat{L}_e V_I^e(t) = K_{IE} S_C[V_E^e(t) - V_E^i(t)], \\ \hat{L}_e V_S^e(t) = K_{SE} S_C[V_E^e(t-\tau) - V_E^i(t-\tau)] + I(t), \\ \hat{L}_i V_S^i(t) = f(p) K_{SR} S_T[V_R^e(t)], \\ \hat{L}_e V_R^e(t) = K_{RE} S_C[V_E^e(t-\tau) - V_E^i(t-\tau)] + K_{RS} S_T[V_S^e(t) - V_S^i(t)], \end{cases} \tag{A.1}$$

which, by neglecting the cortical inhibitory neurons reduce to Eqs. (8).

In the case of constant external input $I(t) = I_0$, the stationary states of Eqs. (A.1) can be obtained by $dV_a^{e,i}/dt = 0$ for $a \in \{E, R, S\}$ leading to

$$\begin{cases} V_E^{*e} = K_{ES} S_T[V_S^{*e} - V_S^{*i}], \\ V_S^{*e} = K_{SE} S_C[V_E^{*e}] + I_0, \\ V_S^{*i} = f(p) K_{SR} S_T[V_R^{*e}], \\ V_R^{*e} = K_{RE} S_C[V_E^{*e}] + K_{RS} S_T[V_S^{*e} - V_S^{*i}]. \end{cases} \tag{A.2}$$

By inserting these equations into each other

$$V_E^{*e} = K_{SE} S_T\left[K_{SE} S_C[V_E^{*e}] + I_0 - f(p) K_{SR} S_T[G[V_E^{*e}]]\right], \tag{A.3}$$

where $G[V_E^{*e}] \equiv K_{RE} S_C[V_E^{*e}] + \dfrac{K_{RS}}{K_{ES}} V_E^{*e}$. Since all the resting states $V_a^{*e,i}$ for $a \in \{E, R, S\}$ can be written as an implicit function of $V_E^{*e}$, the number of solutions of $V_E^{*e}$, i.e., the number of roots of Eq. (A.3), is identical to the number of resting states.

## Appendix B. Theoretical power spectrum

The solution of Eq. (11) system for $t \to \infty$ is

$$\boldsymbol{Y}(t) = \int_{-\infty}^{\infty} \boldsymbol{G}(t - t')\boldsymbol{\xi}(t')dt', \tag{B.1}$$

with the matrix Greens function $\boldsymbol{G} \in \mathcal{R}^{4\times4}$ and substituting Eq. (B.1) into Eq. (11) leads to

$$\hat{\boldsymbol{L}}\left(\frac{\partial}{\partial t}\right)\boldsymbol{G}(t) = \boldsymbol{A}\boldsymbol{G}(t) + \boldsymbol{B}\boldsymbol{G}(t - \tau) + \mathbf{1}\delta(t), \tag{B.2}$$

with the unitary matrix $\mathbf{1} \in \mathbb{R}^{4\times4}$.

Then the Fourier transform of the matrix Greens function

$$\tilde{\boldsymbol{G}}(\nu) = \frac{1}{\sqrt{2\pi}}[\boldsymbol{L}(\nu) - \boldsymbol{A} - \boldsymbol{B}e^{-2\pi i\nu\tau}]^{-1}, \tag{B.3}$$

and the Wiener-Khinchine theorem defines the power spectral density matrix to

$$\boldsymbol{P}(\nu) = 2\kappa\sqrt{2\pi}\tilde{\boldsymbol{G}}(\nu)\tilde{\boldsymbol{G}}^{\top}(-\nu),$$

where the high index $\top$ denotes the transposed matrix. Essentially we assume that the EEG is generated by the activity of pyramidal cortical cells. By virtue of the specific choice of external input to relay neurons, the power spectrum of the EEG just depends on one matrix component of the Greens function by

$$P_E(\nu) = 2\kappa\sqrt{2\pi}\tilde{G}_{1,2}(\nu)\tilde{G}_{1,2}(-\nu) = 2\kappa\sqrt{2\pi}\left|\tilde{G}_{1,2}(\nu)\right|^2. \tag{B.4}$$

In detail, we find $\boldsymbol{Y}(t) = \left(V_E^e(t) - V_E^{*e}, V_S^e(t) - V_S^{*e}, V_S^i(t) - V_S^{*i}, V_R^e(t) - V_R^{*e}\right)^{\top}$, the diagonal matrix $\hat{L}_{11} = \hat{L}_{22} = \hat{L}_{44} = \hat{L}_e(\nu)$, $\hat{L}_{33} = \hat{L}_i(\nu, p)$ and

$$\boldsymbol{A}(p) = \begin{pmatrix} 0 & 0 & 0 & 0 \\ 0 & 0 & 0 & 0 \\ 0 & 0 & 0 & f(p)K_3 \\ 0 & K_5 & -K_5 & 0 \end{pmatrix}, \boldsymbol{B}(p) = \begin{pmatrix} 0 & K_1 & -K_1 & 0 \\ K_2 & 0 & 0 & 0 \\ 0 & 0 & 0 & 0 \\ K_4 & 0 & 0 & 0 \end{pmatrix}$$

with

$$\begin{aligned}
\hat{L}_e(\nu) &= 1 + \frac{2\pi i\nu}{\beta_e} \quad , \quad \hat{L}_i(\nu, p) = 1 + \frac{2\pi i\nu p}{\beta_i^0} \, , \\
K_1 &= K_{ES} \frac{dS_T[V]}{dV} \mid_{V=(V_S^{*e}-V_S^{*i})}, \\
K_2 &= K_{SE} \frac{dS_C[V]}{dV} \mid_{V=V_E^{*e}} \quad , \quad K_3 = K_{SR} \frac{dS_T[V]}{dV} \mid_{V=V_R^{*e}}, \\
K_4 &= K_{RE} \frac{dS_C[V]}{dV} \mid_{V=V_E^{*e}} \quad , \quad K_5 = K_{RS} \frac{dS_T[V]}{dV} \mid_{V=(V_S^{*e}-V_S^{*i})} \, .
\end{aligned}$$

The constants $K_i,\ i = 1, \ldots, 5$ depend on the anaesthetic factor $p$ since they are evaluated at the resting state depending on $p$ itself. Hence

$$\tilde{\boldsymbol{G}}(\nu, p) = \frac{1}{\sqrt{2\pi}} \begin{bmatrix} \hat{L}_e(\nu) & -K_1 e^{-2\pi i\nu\tau} & K_1 e^{-2\pi i\nu\tau} & 0 \\ -K_2 & \hat{L}_e(\nu) & 0 & 0 \\ 0 & 0 & \hat{L}_i(\nu, p) & -f(p)K_3 \\ -K_4 e^{-2\pi i\nu\tau} & -K_5 & K_5 & \hat{L}_e(\nu) \end{bmatrix}^{-1} , \tag{B.5}$$

and

$$\tilde{G}_{1,2}(\nu, p) = \frac{-K_1 \hat{L}_i(\nu, p) e^{-2\pi i\nu\tau}}{\hat{L}_e(\nu)(\hat{L}_e(\nu)\hat{L}_i(\nu, p) + C_2) + e^{-4\pi i\nu\tau}(C_3 - C_1\hat{L}_i(\nu, p))}, \tag{B.6}$$

with $C_1 = K_1K_2$, $C_2 = f(p)K_3K_5$ and $C_3 = f(p)K_1K_3K_4$.

We can rewrite

$$\tilde{G}_{1,2}(\nu, p) = \frac{R_N(\nu, p) + iI_N(\nu, p)}{R_D(\nu, p) + iI_D(\nu, p)}, \tag{B.7}$$

and obtain Eq. (12) with

$$\begin{aligned}
R_N(\nu, p) &= K_1 \left( \cos(2\pi\nu\tau) + \frac{2\pi\nu p}{\beta_i^0} \sin(2\pi\nu\tau) \right), \\
I_N(\nu, p) &= K_1 \left( -\sin(2\pi\nu\tau) + \frac{2\pi\nu p}{\beta_i^0} \cos(2\pi\nu\tau) \right), \\
R_D(\nu, p) &= \frac{-(2\pi\nu)^2}{\beta_e} \left( \frac{1}{\beta_e} + \frac{2p}{\beta_i^0} \right) + C_2 + 1 + (C_3 - C_1)(\cos(4\pi\nu\tau)) - C_1 \frac{2\pi\nu p}{\beta_i^0} \sin(4\pi\nu\tau), \\
I_D(\nu, p) &= \frac{-(2\pi\nu)^3 p}{\beta_e^2 \beta_i^0} + \frac{2\pi\nu}{\alpha}(C_2 + 2) + \frac{2\pi\nu p}{\beta_i^0} - (C_3 - C_1)(\sin(4\pi\nu\tau)) - C_1 \frac{2\pi\nu p}{\beta_i^0} \cos(4\pi\nu\tau).
\end{aligned}$$

## Appendix C. Contribution to power spectrum

Now we parametrize the contribution of PSPs to the power spectrum in the $\delta-$ and $\alpha-$ frequency bands. Substituting the ansatz $\boldsymbol{Y}(t) = e^{\lambda t}\mathbf{u}$ with eigenfunction $\mathbf{u} = [u_E^e, u_S^e, u_S^i, u_R^e]^\top$ into Eq. (11) yields

$$\begin{cases} \left(\frac{\lambda}{\beta_e} + 1\right) u_E^e = K_1(u_S^e - u_S^i)e^{-\lambda\tau}, \\ \left(\frac{\lambda}{\beta_e} + 1\right) u_S^e = K_2 u_E^e e^{-\lambda\tau}, \\ \left(\frac{\lambda}{\beta_i} + 1\right) u_S^i = f(p)K_3 u_R^e, \\ \left(\frac{\lambda}{\beta_e} + 1\right) u_R^e = K_4 u_E^e e^{-\lambda\tau} + K_5(u_S^e - u_S^i). \end{cases} \tag{C.1}$$

Now we can rearrange all the elements of eigenfunction $\mathbf{u}$ in terms of the first element, i.e. $u_E^e$ as

$$\begin{cases} u_E^e = u_1(\lambda)u_E^e, \\ u_S^e = \left(\frac{K_2 e^{-\lambda\tau}}{1 + \frac{\lambda}{\beta_e}}\right) u_E^e \equiv u_2(\lambda)u_E^e, \\ u_S^i = \left(\frac{K_2 e^{-\lambda\tau}}{1 + \frac{\lambda}{\beta_e}} - \frac{1 + \frac{\lambda}{\beta_e}}{K_1 e^{-\lambda\tau}}\right) u_E^e \equiv u_3(\lambda)u_E^e, \\ u_R^e = \frac{1 + \frac{\lambda}{\beta_i}}{f(p)K_3}\left(\frac{K_2 e^{-\lambda\tau}}{1 + \frac{\lambda}{\beta_e}} - \frac{1 + \frac{\lambda}{\beta_e}}{K_1 e^{-\lambda\tau}}\right) u_E^e \equiv u_4(\lambda)u_E^e. \end{cases} \tag{C.2}$$

Then the associated normalized eigenfunction with known eigenvalue $\lambda$ is $\hat{\mathbf{u}} = C\,(1, u_2(\lambda), u_3(\lambda), u_4(\lambda))^\top$ with $C = \dfrac{1}{\sqrt{1 + u_2^2 + u_3^2 + u_4^2}}$. All elements of vector $\boldsymbol{Y}(t) = [y_1(t), y_2(t), y_3(t), y_4(t)]^\top$ can be written as $y_n(t) = \hat{u}_n e^{\lambda t} + \hat{u}_n^* e^{\lambda^* t}$ for $n = 1, ..., 4$. Here the superscript $*$ denotes the complex conjugate. Let $\lambda = \gamma + 2\pi i\nu$ and $\hat{u}_n = R_n + iI_n$, then $y_n(t)$ becomes

$$\begin{aligned} y_n(t) &= (R_n + iI_n)e^{(\gamma + 2\pi i\nu)t} + (R_n - iI_n)e^{(\gamma - 2\pi i\nu)t} \\ &= 2e^{\gamma t}(R_n \cos(2\pi\nu t) - I_n \sin(2\pi\nu t)), \end{aligned} \tag{C.3}$$

and the contribution of excitatory and inhibitory currents to power in a certain frequency $\nu$, in different populations can be defined by Eq. (13).

## References


Alkire, M., Haier, R., Fallon, J., 2000. Toward a unified theory of narcosis: brain imaging evidence for a thalamocortical switch as the neurophysiologic basis of anesthetic-induced unconsciousness. Conscious. Cogn 9, 370–386.

Amari, S., 1977. Dynamics of pattern formation in lateral-inhibition type neural fields. Biol. Cybernetics 27, 77–87.

Antkowiak, B., 2002. In vitro networks: cortical mechanisms of anaesthetic action. Brit. J. Anaesth. 89 (1), 102–111.

Belelli, D., Harrison, N. L., Maguire, J., Macdonald, R. L., Walker, M. C., Cope, D. W., 2009. Extra-synaptic gabaa receptors: form, pharmacology, and function. J. Neurosc. 29 (41), 12757–12763.

Bojak, I., Liley, D., 2005. Modeling the effects of anesthesia on the electroencephalogram. Phys. Rev. E 71, 041902.

Boly, M., Moran, R., Murphy, M., Boveroux, P., Bruno, M. A., Noirhomme, Q., Ledoux, D., Bonhomme, V., Brichant, J. F., Tononi, G., Laureys, S., Friston, K. I., 2012. Connectivity changes underlying spectral eeg changes during propofol-induced loss of consciousness. J. Neurosci. 32 (20), 7082–7090.

Byoung-Kyong, M., 2010. A thalamic reticular networking model of consciousness. Theor Biol Med Model. 7.

Chau, P.-L., 2010. New insights into the molecular mechanisms of general anaesthetics. Br. J. Pharmacol. 161, 288–307.

Ching, S., Cimenser, A., Purdon, P. L., Brown, E. N., Kopell, N. J., 2010. Thalamocortical model for a propofol-induced-rhythm associated with loss of consciousness. Proc. Natl. Acad. Sci. USA 107 (52), 22665–22670.

Ching, S., Purdon, P. L., Vijayand, S., Kopell, N. J., Brown, E. N., 2012. A neurophysiological-metabolic model for burst suppression. Proc. Natl. Acad. Sci. USA 109 (8), 3095–3100.

Cimenser, A., Purdon, P. L., Pierce, E. T., Walsh, J. L., Salazar-Gomez, A. F., Harrell, P. G., Tavares-Stoeckel, C., Habeeb, K., Brown, E. N., 2011. Tracking brain states under general anesthesia by using global coherence analysis. Proc. Natl. Acad. Sci. USA 108 (21), 8832–8837.

Dang-Vu, T., Schabus, M., Desseilles, M., Albouy, G., Boly, M., Darsaud, A., Gais, S., Rauchs, G., Sterpenich, V., Vandewalle, G., Carrier, J., Moonen, G., Balteau, E., Degueldre, C., Luxen, A., Phillips, C., Maquet, P., 2008. Spontaneous neural activity during human slow wave sleep. Proc. Natl. Acad. Sci. USA 105 (39), 15160–15165.

David, O., Friston, K. J., 2003. A neural mass model for meg/eeg: coupling and neuronal dynamics. NeuroImage 20, 1743–1755.

David, O., Kiebel, S. J., Harrison, L. M., Mattout, J., Kilner, J. M., Friston, K. J., 2006. Dynamic causal modeling of evoked responses in eeg and meg. NeuroImage 30, 1255–1272.

Drover, J., Schiff, N., Victor, J., 2010. Dynamics of coupled thalamocortical modules. J. Comput. Neurosci. 28, 605–616.

Farrant, M., Nusser, Z., 2005. Variations on an inhibitory theme: phasic and tonic activation of gabaa receptors. Nature Rev. Neurosci. 6, 215–229.

Feshchenko, V., Veselis, R., Reinsel, R., 2004. Propofol-induced alpha rhythm. Neuropsychobiology 50, 257–266.

Foster, B. L., Bojak, I., Liley, D., 2008. Population based models of cortical drug response: insights from anaesthesia. Cogn. Neurodyn. 2 (4), 283–296.

Franks, N., 2008. From molecular target to neuronal pathways of sleep and arousal. Nature 9, 370–386.

Freestone, D., Aram, P., Dewar, M., Scerri, K., Grayden, D., Kadirkamanathan, V., 2011. A data-driven framework for neural field modeling. NeuroImage 56 (3), 1043–1058.

Garcia, P. S., Kolesky, S. E., Jenkins, A., 2010. General anesthetic actions on gabaa receptors. Curr. Neuropharmacol. 8 (1), 2–9.

Grasshoff, C., Drexler, B., Rudolph, U., Antkowiak, B., 2006. Anaesthetic drugs: linking molecular actions to clinical effects. Curr. Pharm. Des. 12 (28), 3665–3679.

Gugino, L. D., Chabot, R. J., Prichep, L. S., John, E. R., Formanek, V., Aglio, L. S., 2001. Quantitative eeg changes associated with loss and return of consciousness in healthy adult volunteers anaesthetized with propofol or sevoflurane. Br. J. Anaesth. 87, 421–428.

Hazeaux, C., Tisserant, D., Vespignani, H., Hummer-Sigiel, L., Kwan-Ning, V., Laxenaire, M., 1987. Electroencephalographic changes produced by propofol. Ann. Fr. Anesth. Reanim. 6, 261–266.

Hindriks, R., van Putten, M. J. A. M., 2012. Meanfield modeling of propofol-induced changes in spontaneous eeg rhythms. Neuroimage 60, 2323–2344.

Hindriks, R., van Putten, M. J. A. M., 2013. Thalamo-cortical mechanisms underlying changes in amplitude and frequency of human alpha oscillations. Neuroimage 70, 150–163.

Hutt, A., 2012. The population firing rate in the presence of gabaergic tonic inhibition in single neurons and application to general anaesthesia. Cogn. Neurodyn. 6, 227–237.

Hutt, A., 2013. The anaesthetic propofol shifts the frequency of maximum spectral power in eeg during general anaesthesia: analytical insights from a linear model. Front. Comp. Neurosci. 7, 2.

Hutt, A., Buhry, L., 2014. Study of gabaergic extra-synaptic tonic inhibition in single neurons and neural populations by traversing neural scales: application to propofol-induced anaesthesia. J. Comput. Neurosci. in press.

Hutt, A., Longtin, A., 2009. Effects of the anesthetic agent propofol on neural populations. Cogn. Neurodyn. 4 (1), 37–59.

Jirsa, V., Haken, H., 1996. Field theory of electromagnetic brain activity. Phys. Rev. L 77, 960–963.

Johnson, B., Sleigh, J., Kirk, I., Williams, M., 2003. High-density eeg mapping during general anaesthesia with xenon and propofol: a pilot study. Anaesth Intensive Care. 31 (2), 155–163.

Kitamura, A., Marszalec, W., Yeh, J., Narahashi, T., 2002. Effects of halothane and propofol on excitatory and inhibitory synaptic transmission in rat cortical neurons. J. Pharmacol. 304 (1), 162–171.

Kullmann, D. M., Ruiz, A., Rusakov, D. M., Scott, R., Semyanov, A., Walker, M. C., 2005. Presynaptic, extrasynaptic and axonal gabaa receptors in the cns: where and why? Prog. Biophys. Mol. Biol. 87, 33–46.

Lee, U., Oh, G., Kim, S., Noh, G., Choi, B., Mashour, G. A., 2010. Brain networks maintain a scale-free organization across consciousness, anesthesia, and recovery: Evidence for adaptive reconfiguration. Anesthesiology 113 (5), 1081–1091.

Lewis, L., Weiner, V., Mukamel, E., Donoghue, J., Eskandar, E., Madsen, J., Anderson, W., Hochberg, L., Cash, S., Brown, E., Purdon, P., 2012. Rapid fragmentation of neuronal networks at the onset of propofol-induced unconsciousness. Proc Natl Acad Sci USA 109 (21), E3377–3386.

Liley, D., Bojak, I., 2005. Understanding the transition to seizure by modeling the epileptiform activity of general anaesthetic agents. J. Clin. Neurophysiol. 22, 300–313.

Liley, D., Cadusch, P., Dafilis, M., 2002. A spatially continuous mean field theory of electrocortical activity. Network: Comput. Neural Syst. 13, 67–113.

Liley, D., Cadusch, P., Wright, J., 1999. A continuum theory of electrocortical activity. Neurocomp. 26-27, 795–800.

Liley, D., Walsh, M., 2013. The mesoscopic modeling of burst suppression during anesthesia. Front. Comp. Neurosci. 7, 46.

Maquet, P., Degueldre, C., Delfiore, G., Aerts, J., Peters, J., Luxen, A., Franck, G., 1997. Functional neuroanatomy of human slow wave sleep. J. Neurosci. 17 (8), 2807–2812.

Massimini, M., Ferrarelli, F., Huber, R., Esser, S. K., Singh, H., Tononi, G., 2005. Breakdown of cortical effective connectivity during sleep. Science 309, 2228–2232.

McCarthy, M. M., Brown, E. N., Kopell, N., 2008. Potential network mechanisms mediating electroencephalographic beta rhythm changes during propofol-induced paradoxical excitation. J. Neurosci. 28 (50), 13488–13504.

Molaee-Ardekani, B., Senhadji, L., Shamsollahi, M., Vosoughi-Vahdat, B., E.Wodey, 2007. Brain activity modeling in general anesthesia: Enhancing local mean-field models using a slow adaptive firing rate. Phys. Rev. E 76, 041911.

Murphy, M., Bruno, M. A., Riedner, B. A., Boveroux, P., Noirhomme, Q., Landsness, E. C., Brichant, J.-F., Phillips, C., Massimini, M., Laureys, S., Tononi, G., Boly, M., 2011. Propofol anesthesia and sleep: A high-density eeg study. Sleep 34 (3), 283–291.

Nunez, P., 1974. The brain wave equation: A model for the eeg. Math.Biosc. 21, 279–291.

Nunez, P., 1981. Electrical Fields of the Brain. Oxford University Press, Oxford.

Nunez, P., Srinivasan, R., 2006. Electric Fields of the Brain: The Neurophysics of EEG. Oxford University Press, New York - Oxford.

Orser, B., 2006. Extrasynaptic gabaa receptors are critical targets for sedative-hypnotic drugs. J. Clin. Sleep Med. 2, S12–8.

Pinotsis, D., Moran, R., Friston, K., 2012. Dynamic causal modeling with neural fields. NeuroImage 59 (2), 1261–1274.

Purdon, P. L., Pierce, E. T., Mukamel, E. A., Prerau, M. J., Walsh, J. L., Wong, K. F., Salazar-Gomez, A. F., Harrell, P. G., Sampson, A. L., Cimenser, A., Ching, S., Kopell, N. J., Tavares-Stoeckel, C., Habeeb, K., Merhar, R., Brown, E. N., 2012. Electroencephalogram signatures of loss and recovery of consciousness from propofol. Proc. Natl. Acad. Sci. USA 110, E1142–1150.

Rennie, C., Robinson, P., Wright, J., 2002. Unified neurophysical model of eeg spectra and evoked potentials. Biol. Cybern. 86 (6), 457–471.

Robinson, P., C.J.Rennie, D.L.Rowe, S.C.O'Connor, 2004. Estimation of multiscale neurophysiologic parameters by electroencephalographic means. Human Brain Mapping 23, 53–72.

Robinson, P., Rennie, C., Rowe, D., 2002. Dynamics of large-scale brain activity in normal arousal states and eplieptic seizures. Phys. Rev. E 65 (4), 041924.

Robinson, P., Rennie, C., Wright, J., Bahramali, H., Gordon, E., Rowe, D., 2001. Prediction of electroencephalographic spectra from neurophysiology. Phys. Rev. E 63 (2), 1933.

Rudolph, U., Antkowiak, B., 2004. Molecular and neuronal substrates for general anaesthetics. Nat. Rev. Neurosci 5, 709–720.

San-juan, D., Chiappa, K., Cole, A., 2010. Propofol and the electroencephalogram. Clin. Neurophysiol. 121, 998–1006.

Semyanov, A., Walker, M. C., Kullmann, D. M., Silver, R. A., 2004. Tonically active gabaa receptors: modulating gain and maintaining the tone. Trends Neurosc. 27 (5), 262–269.

Siegel, J. M., 2009. Sleep viewed as a state of adaptive inactivity. Nature Rev. Neurosci. 10, 747–753.

Spiegler, A., Kiebel, S., Atay, F., Knosche, T., 2010. Bifurcation analysis of neural mass models: Impact of extrinsic inputs and dendritic time constants. NeuroImage 52 (3), 1041–1058.

Spiegler, A., Knosche, T., Schwab, K., Haueisen, J., Atay, F., 2011. Modeling brain resonance phenomena using a neural mass model. PLoS Comput. Biol. 7 (12), e1002298.

Steriade, M., Contreras, D., Curro Dossi, R., Nunez, A., 1993. The slow ($<$ 1 hz) oscillation in reticular thalamic and thalamocortical neurons: scenario of sleep rhythm generation in interacting thalamic and neocortical networks. J. Neurosci. 13 (8), 3284–3299.

Steyn-Ross, M., Steyn-Ross, D., Sleigh, J., 2004. Modelling general anaesthesia as a first-order phase transition in the cortex. Prog. Biophys. Molecul. Biol. 85 (2-3), 369–385.

Steyn-Ross, M., Steyn-Ross, D., Sleigh, J., Wilcocks, L., 2001a. Toward a theory of the general-anesthetic-induced phase transition of the cerebral cortex: I. a thermodynamic analogy. Phys. Rev. E 64, 011917.

Steyn-Ross, M., Steyn-Ross, D., Sleigh, J., Wilcocks, L., 2001b. Toward a theory of the general-anesthetic-induced phase transition of the cerebral cortex: Ii. numerical simulations, spectra entropy, and correlation times. Phys. Rev. E 64, 011918.

Steyn-Ross, M., Steyn-Ross, D., Sleigh, J. W., Liley, D. T. J., 1999. Theoretical electroencephalogram stationary spectrum for a white-noise-driven cortex: Evidence for a general anesthetic-induced phase transition. Phys. Rev. E 60 (6), 7299–7311.

Vanini, G., Baghdoyan, H., 2013. Extrasynaptic gabaa receptors in rat pontine reticular formation increase wakefulness. Sleep 36 (3), 337–343.

Victor, J., Drover, J., Conte, M. M., Schiff, N., 2011. Mean-field modeling of thalamocortical dynamics and a model-driven approach to eeg analysis. Proc. Natl. Acad. Sci. USA 118, 15631–15638.

Vijayan, S., Ching, S., Cimenser, A., Purdon, P. L., Brown, E. N., Kopell, N. J., 2013. Thalamocortical mechanisms for the anteriorization of alpha rhythms during propofol-induced unconsciousness. J. of Neurosc. 33 (27), 11070–11075.

Wieloch, T., Nikolich, K., 2006. Mechanisms of neural plasticity following brain injury. Current Opinion in Neurobiology 16 (3), 258–264.

Wilson, H., Cowan, J., 1973. A mathematical theory of the functional dynamics of cortical and thalamic nervous tissue. Kybernetik 13, 55–80.

Wilson, M., Sleigh, J., Steyn-Ross, A., Steyn-Ross, M., 2006. General anesthetic-induced seizures can be explained by a mean-field model of cortical dynamics. Anesthsiol. 104 (3), 588–593.

Ying, S., Goldstein, P., 2001. Propofol effects on the thalamus: Modulation of gabaergic synaptic inhibition and suppression of neuronal excitability. Abstract Viewer/Itinerary Planner Washington, DC: Society for Neuroscience 89 (411).

Ying, S., Goldstein, P., 2005a. Propofol-block of SK channels in reticular thalamic neurons enhances gabaergic inhibition in relay neurons. J. Neurophysiol. 93, 1935–1948.

Ying, S., Goldstein, P., 2005b. Propofol suppresses synaptic responsiveness of somatosensory relay neurons to excitatory input by potentiating gabaa receptor chloride channels. Mol. Pain 1, 2.

Zhou, C., Liu, J., Chen, X., 2012. General anesthesia mediated by effects on ion channels. World Journal of Critical Care Medicine 1, 80–93.